

**University of Alberta**

Analysis and synthesis of strongly coupled optical microring resonator  
networks

by

Alan Cheng-Lun Tsay

A thesis submitted to the Faculty of Graduate Studies and Research  
in partial fulfillment of the requirements for the degree of

Master of Science

in

Photonics and Plasmas

Electrical and Computer Engineering

©Alan Cheng-Lun Tsay

Fall 2011

Edmonton, Alberta

Permission is hereby granted to the University of Alberta Libraries to reproduce single copies of this thesis and to lend or sell such copies for private, scholarly or scientific research purposes only. Where the thesis is converted to, or otherwise made available in digital form, the University of Alberta will advise potential users of the thesis of these terms.

The author reserves all other publication and other rights in association with the copyright in the thesis and, except as herein before provided, neither the thesis nor any substantial portion thereof may be printed or otherwise reproduced in any material form whatsoever without the author's prior written permission.

Dedication

To Wendy

Thank you for your love and encouragements

# Abstract

Integrated photonics have received much attention in recent years as there is a concerted effort towards achieving Very-Large-Scale-Integration of optical components. One of the key elements enabling such dense integration is the optical microring resonator, which has found pervasive applications in integrated optics due to its ultrahigh quality factor and highly dispersive spectral characteristics. Recently it was shown that two dimensionally coupled microring resonators (2D-CMRs) can be used to realize advanced optical transfer functions, making them highly attractive for spectral engineering applications. Existing methods for analysis and design of 2D-CMR networks based on the energy coupling formalism are limited to narrowband devices due to its inherent weak coupling assumptions. This thesis develops rigorous field coupling methods for analyzing and synthesizing general 2D-CMR networks in the strong coupling regime, which exhibit novel physical phenomena not previously observed. Advanced applications of strongly coupled CMR networks are also proposed for broadband applications.

# Acknowledgements

I would like to offer my deepest gratitude to my supervisor, Dr. Vien Van, for his patient guidance, supervision, and the opportunity for the project. I want to extend my appreciation to Ashok Prabhu Masilamani for excellent insights given on various subjects, and also thank my fellow members at NPRL, Siamak Abdhullahi, Rice Mi, David Perron, Ken Lei, Cameron Horvath, and Daniel Bachman, for their support and making the lab a great place to work in. I want to thank my parents for the early education and let me grow up in a comfortable environment. Finally and most importantly, I want to thank Wendy, for granting me the courage and making everything possible.

This work was supported by Natural Sciences and Engineering Research Council, Alberta Innovates, and various scholarships from University of Alberta.

# Table of Contents

Chapter 1 Introduction .....	1
1.1 Optical microring resonators.....	2
1.2 Microring optical filter architectures .....	3
1.3 Theoretical treatments of microring resonators .....	6
1.4 Objectives .....	7
1.5 Thesis organization .....	7
Chapter 2 Energy Coupling Analysis of Microring Resonators .....	9
2.1 Coupled waveguides .....	9
2.2 Energy coupling in time description of microring resonators.....	11
2.2.1 Transfer function of a single microring resonator.....	11
2.3 Spectral characteristics of a microring resonator.....	14
2.3.1 Resonance condition .....	14
2.3.2 Full width at half maximum (FWHM) bandwidth.....	15
2.3.3 Free Spectral Range (FSR) .....	16
2.3.4 Finesse (F).....	17
2.3.5 Quality factor (Q).....	17
2.4 Energy coupling analysis of 2D coupled microring resonators .....	17
2.5 Summary .....	21
Chapter 3 Field Coupling Analysis of Coupled Microring Resonators .....	22
3.1 Field coupling formalism.....	22
3.1.1 Through-port and drop-port transfer functions .....	29
3.1.2 2D-CMRs with no external bus waveguides .....	32
3.1.3 Direct and indirect coupling-angle matrices .....	33
3.2 Example of a 3×3 2D-CMR.....	36
3.3 Similarity transformations of the field coupling matrix .....	40
3.4 Relationship between energy and field coupling formulations.....	44
3.5 Summary .....	46
3.6 Appendix – Proof of the Circular Property of the Field Coupling Matrices.....	48
Chapter 4 CMR Filter Synthesis Using Field Coupling Formalism .....	50
4.1 General 2D-CMR field coupling synthesis.....	51
4.1.1 Description of the CMR network.....	51
4.1.2 Field coupling synthesis of CMR networks.....	57

4.1.3 Constructing the coupling matrix $M$ .....	59
4.1.4 Determining the CMR network topology and coupling coefficients .....	61
4.1.5 Design example: a 6 <sup>th</sup> -order optical filter .....	62
4.2 Synthesis of $2 \times N$ CMRs by network order reduction .....	63
4.2.1 Description of the $2 \times N$ CMR network .....	64
4.2.2 Network order reduction .....	66
4.2.3 A design example .....	70
4.3 Summary .....	72
Chapter 5 Conclusions .....	73
5.1 Major contributions .....	74
5.2 Recommendations for future works .....	74
Bibliography .....	76

# List of Figures

1.1	Schematic of single microring add/drop filter .....	2
1.2	Common high order microring filter architectures, showing serial coupling (a), parallel coupling (b), and microring loaded Mach-Zehnder schemes.. .....	4
1.3	Schematic of a general 2D-CMR network consisting of coupled microrings arranged in a square lattice .....	5
2.1	Schematic of a coupling junction between waveguide 1 and 2. ....	10
2.2	Single microring resonator add/drop filter.....	12
2.3	Typical spectral response of single microring resonator add/drop filter at through port (solid) and drop port (dashed), showing various spectral properties ..	15
2.4	General schematic of a 2-D array of $N$ mutually coupled microring resonators. ....	18
3.1	Schematic of a general 2D-CMR structure consisting of an $n \times m$ array of $N$ coupled microring resonators.....	23
3.2	Example of coupled microring triplets that would give rise to counter-propagation waves .....	23
3.3	(a) Equivalent unfolded coupled-waveguide array of a general 2D-CMR. (b) “Stacked-rings” schematic of a 2D-CMR characterized by field coupling matrix $\mathbf{M}$ and extrinsic loss matrix $\mathbf{L}$ . ....	25
3.4	Special case of a quadruplet CMR network arranged in $2 \times 2$ square (a), and its corresponding field coupling matrices (b).....	36
3.5	(a) $3 \times 3$ 2D-CMR structure. (b) Unfolded coupled-waveguide array. (c) and (d) Magnitudes of the elements of the direct and indirect coupling matrices of the strongly-coupled CMR structure.....	37
3.6	Drop-port response of the $3 \times 3$ 2D-CMR under (a) weak coupling and (b) strong coupling conditions. In (a), results were computed using field coupling (solid black line) and energy coupling (dashed grey line). In (b), results were computed using field coupling with (solid grey line) and without (solid black line) indirect coupling matrix $\mathbf{X}$ . Energy coupling result is shown by dashed grey line. In (c) drop port response in the strong coupling case is calculated using field coupling with 1% round-trip loss.....	38
3.7	Pole-zero diagram of the $3 \times 3$ 2D-CMR under strong coupling condition computed (a) without and (b) with the indirect coupling matrix $\mathbf{X}$ . ....	40
3.8	Generation of a new microring coupling topology by similarity transformation	

of the coupling-angle matrix: (a) original coupling topology; (b) transformed coupling topology. The direct coupling-angle matrix $\Psi$ of each topology is also shown.....	42
3.9 Drop-port and through-port spectral responses of the CMR structure in Figure 6(a) (solid lines) and Figure 6(b) (dashed lines).....	43
4.1 (a) Schematic of a general 2D coupled microring array with $N$ microrings; (b) inner CMR network. ....	51
4.2 (a) Target filter responses (dashed lines) and responses of the synthesized CMR network (solid lines). (b) Polynomials of the transfer functions of the target filter. (c) Coupling-angle matrix and (d) coupling topology of the synthesized CMR network. ....	62
4.3 Schematic of a $2 \times N$ CMR network and its depiction as a cascade of $N$ stages of microring pairs. ....	65
4.4 (a) Target (grey dotted lines) and synthesized (black solid lines) filter responses at the drop port ( $ S_{21} ^2$ ) and through port ( $ S_{11} ^2$ ). Grey solid lines show the group delay responses. (b) Schematic and coupling parameters of the synthesized CMR network.....	71

## List of Tables

4.1 Coefficients of the transfer polynomials of the target filter response.....	71
---	----

# List of Symbols

$\kappa$	Field coupling coefficient
$\tau$	Field transmission coefficient
$s_i, s_t, s_a, s_d$	Signals at input, through, add, drop port
$\mu$	Energy coupling coefficient
$T_{rt}$	Round-trip time
$R$	Radius of the microring
$v_g$	Group velocity
$\lambda_g$	Guided wavelength
$\omega$	Angular frequency
$\omega_o$	Resonant frequency of microring resonator
$\tau_c$	Cavity amplitude decay time-constant
$\tau_l$	Cavity amplitude decay time-constant due to intrinsic loss
$n_{eff}$	Effective refractive index of a medium
$n_g$	Group refractive index of a medium
$c$	Speed of light in vacuum
$Q$	Quality factor
$z^{-1}$	Round-trip delay variable
$\phi_{rt}$	Round-trip phase
$\mathbf{M}$	Coupling matrix
$\Psi$	Direct coupling angle matrix
$\mathbf{X}$	Indirect coupling angle matrix

# Chapter 1

## Introduction

The last decade has seen an explosive growth in digital communications as the average user data consumption has significantly expanded compared to years before. Data transmissions through optical channels have long since become an inseparable part in communications due to its extreme high capacity and speed compared to electrical systems. However, implementations of bulk optical information signal processing systems are clumsy and difficult to scale up, so miniaturization and integration has become an important drive in the development of more practical optical networks as it proved to be the key that enabled the electronics to be used in countless applications as we see today. Thus the field of integrated photonics was born from this need to allow VLSI integration of many optical components to achieve high level of functionalities on a single chip.

Coupled microring resonators (CMR) are promising building blocks for integrated optics due to their versatile spectral characteristics which can be designed to meet desired specifications. These devices have especially received attention in spectral and dispersion engineering applications such as optical filters [1], slow light [2], optical delay lines [3], coupled-resonator induced transparency [4]. Recently it has been shown that coupled microring resonators of two dimensional (2D) coupling topologies exhibit much richer spectral characteristics than 1D coupling topologies [5], and can be used to realize many general high

order optical transfer functions not realizable by 1D topologies [6]. As the 2D coupling architectures open up more design possibilities of coupled microring devices, it is important to develop rigorous and accurate methodologies for analyzing and designing these devices.

## 1.1 Optical microring resonators

A microring resonator is essentially a waveguide bent in a closed loop, such as a circle, ellipse, or racetrack, and behaves as a whispering gallery mode travelling-wave resonator. Signals from the input waveguide (or bus) are typically coupled to the resonator through evanescent coupling which occurs when the evanescent fields outside the waveguides begin to overlap and result in energy transfer. As the waveguide is bent into a closed loop, signals will resonate in the ring if its round-trip phase is an integral multiple of  $2\pi$ , which results in constructive interference of the signal with itself and a build up of stored energy in the resonator. One of the simplest devices we could achieve

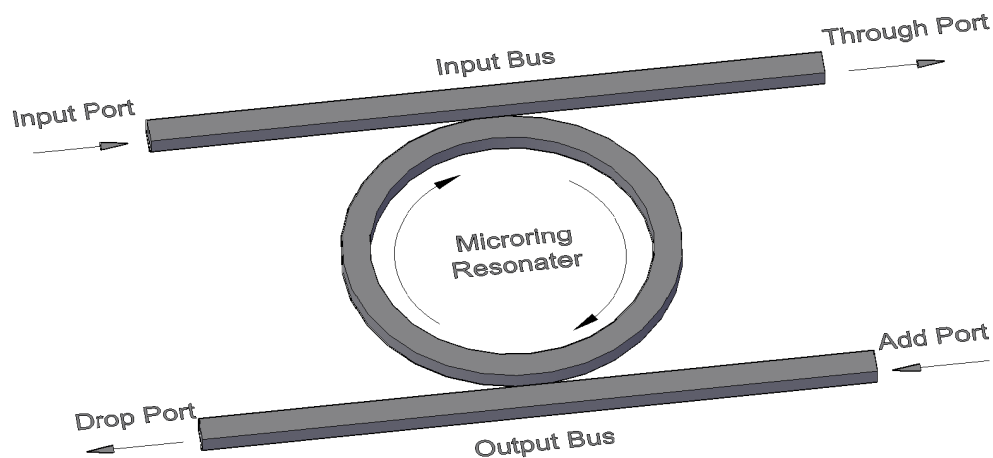


Figure 1.1 – Schematic of single microring add/drop filter

exploiting this property is an add/drop filter as seen in Figure 1.1. When a spectrum of wavelength-division multiplexed (WDM) signals is applied to the input port, only the signal satisfying the resonance condition will resonate in the microring and be eventually transmitted or “dropped” at the drop port, while the rest of the signals will pass on to the through port. Another signal of the same resonance wavelength could also be “added” to the WDM spectrum in the input bus by feeding it from the add port. In practice, however, WDM add/drop filters require stringent spectral characteristics that cannot be met by a single microring resonator and higher order filter architectures with multiple coupled microring resonators are generally used in order to achieve better filter response.

## **1.2 Microring optical filter architectures**

Different architectures of high order microring optical filters have been proposed in the past, such as the microring-loaded Mach-Zehnder interferometer topologies [7, 8], the serial coupling topology [1,9,10], the parallel cascaded array topology [11,12], the two dimensional coupling topology [5,13], and even the dual mode reflection filter topology [14]. Serially coupled microring resonators, as shown in Figure 1.2(a), often referred to as Coupled Resonator Optical Waveguides (CROWs), have received the most attention due to their simple structures for both analysis and design. However, the serial coupling microring topology cannot be used to realize transfer functions with transmission zeros, which limits its spectral performance so that the filter might not be able to meet the sharp skirt roll-off and high out-of-band rejection requirements for Dense Wavelength Division Multiplexing (DWDM) applications [5]. While the

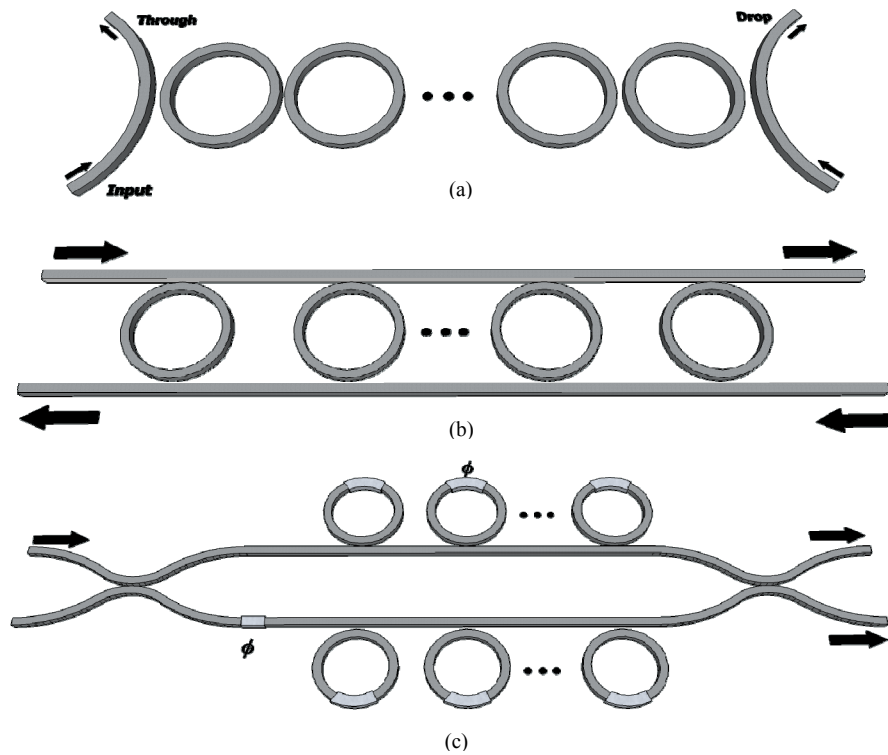


Figure 1.2 – Common high order microring filter architectures, showing serial coupling (a), parallel coupling (b), and microring loaded Mach-Zehnder schemes.

parallel cascaded microring array scheme (Figure 1.2(b)) could realize transmission zeros, its design is more complicated as the poles of the filter cannot be independently controlled. The microring-loaded Mach-Zehnder scheme (Figure 1.2(c)) is based on the sum and difference of two all pass filters in the two arms of the interferometer, and can be used to realize arbitrary poles and transmission zeros with simple design. However, it requires the implementation of individual phase shifters on each of the microring resonators. Recently it has been shown that the microring-loaded Mach-Zehnder structure can be converted into a parallel cascade of double-microrings to simplify its implementation, requiring only one phase shift [15].

Of the various microring filter architectures described above, the two

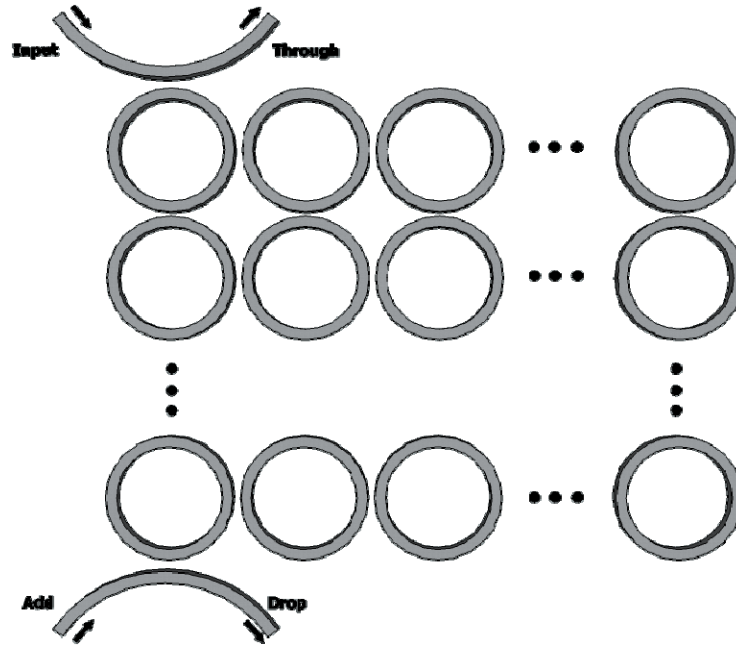


Figure 1.3 – Schematic of a general 2D-CMR network consisting of coupled microrings arranged in a square lattice

dimensionally coupled microring resonator network (shown in Figure 1.3) is the most compact architecture that can be used to achieve various advanced filter transfer functions. The structure consists of synchronously tuned microring resonators (of the same resonance frequency) arranged in a two dimensional square lattice, creating a compact and versatile structure that can be used to realize rich spectral characteristics by adjusting the coupling strengths between the resonators. However, due to the complexity of the structure, the analysis and design of 2D CMR filters have been restricted to narrowband approximations based on the energy coupling formalism. The lack of more rigorous and general analysis and synthesis methodologies limits the usefulness of the 2D CMR architecture in more advanced applications.

### 1.3 Theoretical treatments of microring resonators

Analysis of coupled microring resonators is typically performed in terms of either energy coupling in time or field coupling in space. The energy coupling formalism is strictly valid only for weakly-coupled CMRs where the field circulating in each microring is assumed to be uniform, so that each resonator can be conveniently described by its total stored energy. Energy transfer among the microrings is described by a simple coupled mode equation in time, enabling analytic solutions of the device transfer functions to be obtained and direct filter synthesis method to be developed [5,6]. However, the restriction of weak coupling means that the energy coupling formalism is applicable only for narrow-band CMRs. For strongly-coupled microring resonators, which are characterized by having a bandwidth that is a significant fraction of the free spectral range (FSR) of the microrings, an accurate analysis must be performed based on field coupling in space. However, the field coupling analysis is complicated by the fact that in strongly-coupled CMRs, the field in each microring is not uniform but depends on the positions of the microring coupling junctions. Typically a field-coupling matrix equation is needed to describe each coupling junction, resulting in a large system of matrix equations that generally do not admit analytical solutions or offer physical insight into the characteristics of the device. Thus, although the field coupling formalism has been used to analyze relatively simple structures such as CROWs [9,16] and parallel-cascaded microring resonators [13,17], its application to general 2D microring coupling topologies [18,19] is less popular because the lack of a systematic formulation

makes the analysis cumbersome and tedious. It should be noted that other approaches such as tight binding [20] and Mason's rule in flow-graph theory [21] are also possible, but their applications are restricted to periodic microring structures in the former case and simple coupling topologies in the latter case due to the complexity of the approach.

## **1.4 Objectives**

The objective of this thesis is to develop rigorous analysis and synthesis methodologies based on the field coupling formalism for general two dimensional coupled microring resonator networks. A systematic formulation achieved by transforming a general 2D-CMR structure into an equivalent coupled waveguide array will be presented. The formulation yields closed form expressions for the transfer functions of a 2D CMR network in the strong coupling regime. The relationship between the presented field coupling formalism and the traditional energy coupling formalism will also be derived. The analysis of CMR structures in the strong coupling regime also allows new physics to be uncovered, such as indirect coupling induced transparency. A synthesis method based on the field coupling formalism is also developed, which can be used to design strongly coupled CMR structures with broadband characteristics.

## **1.5 Thesis organization**

This thesis is organized as follows. The theoretical background of microring resonator filters is discussed in Chapter 2, with a review of the analysis approach of the device based on energy coupling formalism. Chapter 3

highlights our work on the development of a general 2D CMR network analysis method based on the field coupling formalism. Chapter 4 presents two methods of the direct synthesis of 2D CMR networks for realizing prescribed optical transfer functions, one based on the inverse procedure of the analysis technique presented in Chapter 3, and the other based on the network order reduction method for designing a  $2 \times N$  network. Finally, Chapter 5 concludes the thesis highlighting key contributions of the work.

# **Chapter 2**

## **Energy Coupling Analysis of**

### **Microring Resonators**

This chapter reviews the basic theory of microring resonators based on the energy coupling formalism. The transfer functions and fundamental characteristics of microring resonators are discussed.

#### **2.1 Coupled waveguides**

In recent years, rectangular dielectric waveguides are of major interest in the photonic research field due to its simple structure, ease of fabrication and potential to be integrated on many platforms. These waveguides are typically designed to operate under the single mode condition (for each dominant polarization). Energy transfer between two dielectric waveguides can be achieved by bringing them close to each other. The evanescent tail extending outside the core of each waveguide would start interacting with each other, resulting in the fields being “coupled”. Evanescent power transfer between two coupled waveguides has been well studied through the Coupled Mode Theory [22,23].

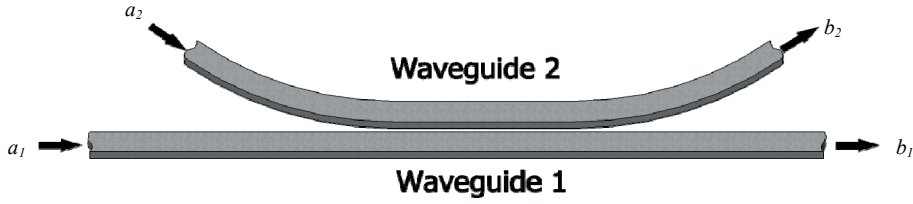


Figure 2.1 – Schematic of a coupling junction between waveguide 1 and 2.

Consider a lossless coupling junction between waveguides 1 and 2 as shown in Figure 2.1. The fields entering the junction in each waveguide are denoted as complex field variables (i.e. include amplitude and phase)  $a_1$  and  $a_2$  and the fields exiting the junction are denoted as  $b_1$  and  $b_2$ . Coupled mode theory yields the following coupling matrix equation relating the output fields to the input fields:

$$\begin{bmatrix} b_1 \\ b_2 \end{bmatrix} = \begin{bmatrix} \tau & -j\kappa \\ -j\kappa & \tau \end{bmatrix} \begin{bmatrix} a_1 \\ a_2 \end{bmatrix}. \quad (2.1)$$

In the above equation,  $\tau$  represents the field transmission coefficient,  $\kappa$  represents the field coupling coefficient, and the factor  $-j$  represents the  $\pi/2$  phase change experienced by the coupled fields. The coupling junction itself is assumed to have zero physical length in the model, so there would be no phase shift in the transmitted fields, and the coupling and transmission coefficients are real. Power conservation is maintained by requiring the two coefficients to be related by,

$$\tau^2 + \kappa^2 = 1. \quad (2.2)$$

## 2.2 Energy coupling in time description of microring resonators

One of the most successful methods for analyzing systems of coupled resonators is the energy coupling in time formalism. This method has been used to analyse coupled microring resonators in 1D [10] and 2D coupling topologies [5]. In this approach, each microring resonator is considered as a lumped oscillator and energy transfer among the resonators is described by a system of coupled mode equations in time. Analytic solutions of the system of equations allow closed form expressions for the transfer functions of the microring networks to be obtained. Filter synthesis methods based on the energy coupling formalism have also been developed for 1D and 2D coupled microring topologies [5,6]. Below we review the analysis approach of microring resonators using the energy coupling formalism.

### 2.2.1 Transfer function of a single microring resonator

To better demonstrate the analysis approach based on the energy coupling formalism, we will analyse the basic single microring add/drop filter configuration and obtain formulas describing its spectral responses [10]. Consider the structure in Figure 2.2, where a single microring resonator of radius  $R$  is evanescently side coupled to a pair of bus waveguides acting as input/output ports. The optical energy wave amplitudes guided in the input, through, add, and drop ports are denoted as  $s_i$ ,  $s_t$ ,  $s_a$ , and  $s_d$ , such that the square modulus ( $|s_i|^2$ ,  $|s_t|^2$ ,  $|s_a|^2$ , and  $|s_d|^2$ ) is the energy of the signal in each respective port. The input and output energy coupling coefficients,  $\mu_i$  and  $\mu_o$ , denote the rates of

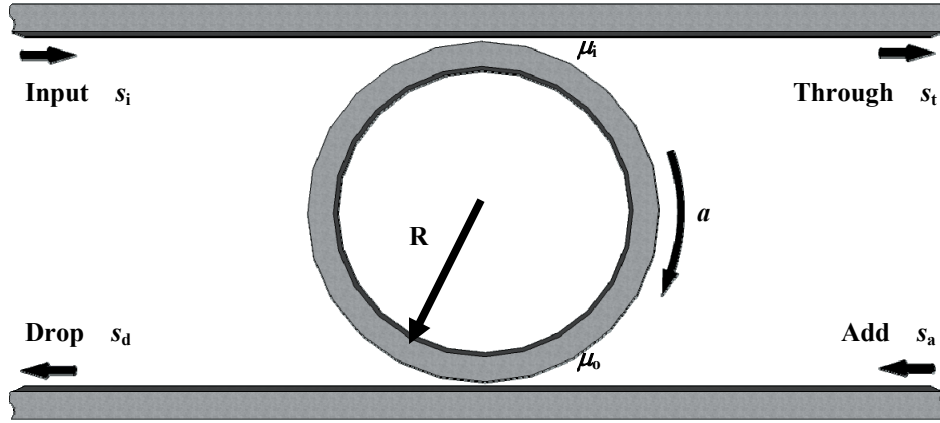


Figure 2.2 – Single microring resonator add/drop filter

energy that gets coupled between the microring and the bus waveguides, and can be related to the field coupling coefficients,  $\kappa$ , mentioned earlier as [5]:

$$\mu^2 = \frac{\kappa^2}{T_{rt}} = \frac{\kappa^2}{2\pi R/v_g} \quad (2.3)$$

where  $T_{rt}$  is the round-trip time it takes the signal travelling at group velocity,  $v_g$ , to travel around the microring of radius  $R$ . The microring resonator is considered as a lumped oscillator with energy signal amplitude  $a(t)$  (such that its stored energy is  $|a(t)|^2$ ) with resonant angular frequency of  $\omega_o$  and cavity amplitude decay time-constant of  $\tau_c$ . The total decay rate includes the effects of energy loss due to external coupling to the input ( $1/\tau_i$ ) and output ( $1/\tau_o$ ) bus waveguides as well as intrinsic loss ( $1/\tau_l$ ) according to

$$1/\tau_c = 1/\tau_i + 1/\tau_o + 1/\tau_l. \quad (2.4)$$

The intrinsic loss in the microring resonator includes bending loss, material absorption, and surface roughness scattering. By considering the energy flows in and out of the resonator, the stored energy in the microring changes with respect

to time according to

$$\frac{d}{dt}a = \left( j\omega_o - \frac{1}{\tau_c} \right) a - j\mu_i s_i . \quad (2.5)$$

Assuming an input signal with harmonic time dependence  $s_i \sim \exp(j\omega t)$ , we can find from (2.5)

$$a = \frac{-j\mu_i}{j(\omega - \omega_o) + \frac{1}{\tau_c}} s_i . \quad (2.6)$$

The drop port and through port signals are related to the energy signal in the microring as

$$\begin{aligned} s_d &= -j\mu_o a, \\ s_t &= s_i - j\mu_i a. \end{aligned} \quad (2.7)$$

Using equations (2.6), (2.7) and setting  $s = j(\omega - \omega_o)$  we can express the drop and through port responses of the filter in terms of the input signal as:

$$s_d = -\frac{\mu_i \mu_o}{s + \frac{1}{\tau_c}} s_i , \quad (2.8a)$$

$$s_t = \frac{s + \frac{1}{\tau_c} - \mu_i^2}{s + \frac{1}{\tau_c}} s_i . \quad (2.8b)$$

The energy coupling coefficients  $\mu_i$  and  $\mu_o$  are related to the decay rates  $1/\tau_i$  and  $1/\tau_o$ , as: [10]

$$\frac{1}{\tau_i} = \frac{\mu_i^2}{2} ; \quad \frac{1}{\tau_o} = \frac{\mu_o^2}{2} . \quad (2.9)$$

Using the above results, we can obtain the following expressions for the through-port and drop-port transfer functions of the single microring resonator add/drop filter as:

$$T_d(s) = \frac{s_d}{s_i} = -\frac{\mu_i \mu_o}{s + \frac{1}{\tau_l} + \mu_i^2 + \mu_o^2}, \quad (2.10a)$$

$$T_t(s) = \frac{s_t}{s_i} = \frac{s + \frac{1}{\tau_l} - \mu_i^2 + \mu_o^2}{s + \frac{1}{\tau_l} + \mu_i^2 + \mu_o^2}. \quad (2.10b)$$

The above energy coupling analysis is strictly valid only for a weakly-coupled (or narrow-band) microring resonator where the field circulating in the microring is assumed to be uniform, so that the resonator can be conveniently described by its total stored energy in this model. This formalism leads to a description of the resonator in the complex frequency  $s$ -domain as in equations (2.10), and is equivalent to the approach commonly used to analyze low-frequency resonators such as microwave cavities and electrical oscillators.

## 2.3 Spectral characteristics of a microring resonator

Microring resonators exhibit spectral characteristics similar to standing-wave oscillators. They are typically characterized by their resonant frequencies, spectral line widths, free spectral range (FSR), finesse (F), and quality factor (Q).

### 2.3.1 Resonance condition

Figure 2.3 shows the simulated spectral response of a typical single microring resonator add/drop filter. The microring is resonating whenever the

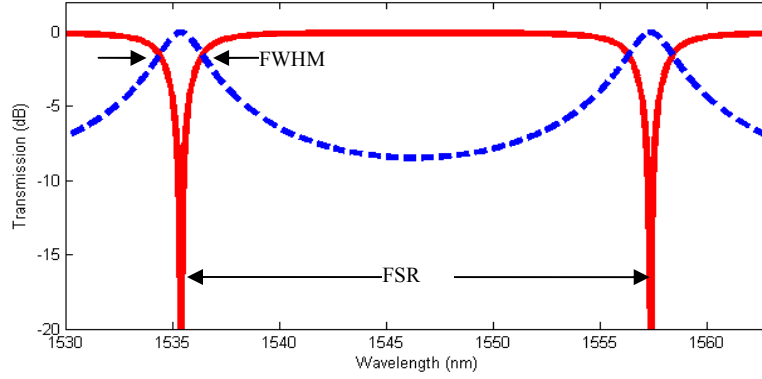


Figure 2.3 – Typical spectral response of single microring resonator add/drop filter at through port (solid) and drop port (dashed), showing various spectral properties

field guided in the ring is in constructive interference with itself after travelling around the microring, which can be described by the following resonance condition:

$$m\lambda_g = 2\pi R \quad (2.11a)$$

where  $m$  is an integer (called the resonance mode number),  $\lambda_g$  is the guided wavelength, and  $R$  is the microring radius. The above condition can also be expressed in terms of frequency as

$$2\pi m = \omega T_{rt} \quad (2.11b)$$

where  $\omega$  is the angular frequency and  $T_{rt}$  is the microring round-trip time. In the add/drop configuration, the resonant condition indicates the wavelength location of the peak transmission at the drop port (dashed curve in Figure 2.3) and the transmission dip at the through port (solid curve).

### 2.3.2 Full width at half maximum (FWHM) bandwidth

Assuming a symmetric structure (equal input and output coupling

coefficients) with no loss, we can solve for the FWHM bandwidth of the single ring add/drop filter as follows. First by squaring Equation (2.10a) and equating it to 1/2 we obtain:

$$\left| \frac{s_d}{s_i} \right|^2 = \left| \frac{-\mu^2}{j\Delta\omega_{1/2} + \mu^2} \right|^2 = \frac{\mu^4}{\Delta\omega_{1/2}^2 + \mu^4} = \frac{1}{2}. \quad (2.12)$$

Solving for  $\Delta\omega_{1/2}$ , the FWHM could then be found as:

$$FWHM = 2\Delta\omega_{1/2} = 2\mu^2. \quad (2.13)$$

The FWHM bandwidth could also be derived based on the field coupling formalism which yields the expression [10]

$$FWHM = \frac{\kappa^2 c}{\pi R n_{eff}} \quad (2.14)$$

where  $n_{eff}$  is the effective index of the microring waveguide,  $c$  is the speed of light in vacuum. We can confirm that the two expressions are the same if  $n_{eff} = n_g$  by using Equation (2.3).

### 2.3.3 Free Spectral Range (FSR)

The spacing between two consecutive resonant peaks is referred to as the free spectral range (FSR) of the resonator, and can be found from (2.11b)

$$FSR_{frequency} = \omega_{m+1} - \omega_m = \frac{2\pi}{T_{rt}} = \frac{c}{Rn_g} \quad (2.15)$$

where  $n_g$  is the group index of the microring waveguide.

### 2.3.4 Finesse (F)

Similar to Fabry-Perot resonators, we can find the finesse (F) of a microring resonator, which is defined as the ratio of the FSR to its resonance width, as

$$F = \frac{FSR_{\omega}}{\Delta\omega} = \frac{\pi}{\kappa^2}. \quad (2.16)$$

The above expression assumes  $n_g = n_{\text{eff}}$ . The figure of finesse represents the ability of a cavity to resolve spectral lines; in terms of WDM filter applications it represents the number of frequency channels that can be accommodated within one FSR.

### 2.3.5 Quality factor (Q)

The quality factor of a resonator commonly defined as

$$Q = \omega_o \frac{\text{Stored Energy}}{\text{Power loss}} \quad (2.17)$$

where  $\omega_o$  is the resonance frequency, can be found for the microring resonator of negligible internal loss as

$$Q = \frac{\omega_o}{\Delta\omega} = \frac{\omega_o \pi R n_{\text{eff}}}{\kappa^2 c}. \quad (2.18)$$

The higher the quality factor, the better the resonator behaves as an energy storage device, and the sharper its resonance peaks are.

## 2.4 Energy coupling analysis of 2D coupled microring resonators

The energy coupling formalism can also be used to analyze more complicated two dimensional coupled microring structures, such as the one shown

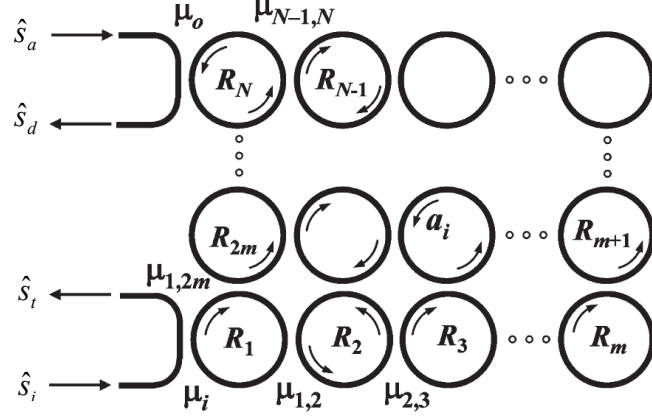


Figure 2.4 - General schematic of a 2-D array of  $N$  mutually coupled microring resonators. [5]

in Figure 2.4. Each microring resonator  $R_k$ ,  $k = 1$  to  $N$ , in the structure has resonant frequency  $\omega_k$ , such that the frequency detune from the center frequency ( $\Delta\omega_k = \omega_k - \omega_0$ ) is small and the microrings could be assumed to have the same intrinsic cavity lifetime  $\tau_c$ . Time harmonic optical signals  $\hat{s}_i$ ,  $\hat{s}_t$ ,  $\hat{s}_a$ , and  $\hat{s}_d$ , denote the energy wave amplitudes at the input, through, add, and transmitted ports. The rate of energy coupling between adjacent microrings  $i$  and  $j$  is denoted by the energy coupling coefficient  $\mu_{i,j}$ . Microrings 1 and  $N$  are also coupled to the input and output waveguides via the corresponding input and output energy coupling coefficients  $\mu_i$  and  $\mu_o$ . Denoting  $\hat{a}_k(t)$  as the energy amplitude stored in microring  $k$ , we can write the system of equations describing the flow of energy in the network similar to equation (2.5) as: [24]

$$\frac{d}{dt} \begin{bmatrix} \hat{a}_1 \\ \hat{a}_2 \\ \vdots \\ \hat{a}_N \end{bmatrix} = \begin{bmatrix} (j\omega_1 - 1/\tau_i) & -j\mu_{1,2} & \cdots & -j\mu_{1,N} \\ -j\mu_{1,2} & (j\omega_2 - 1/\tau_c) & \cdots & -j\mu_{2,N} \\ \vdots & \vdots & \ddots & \vdots \\ -j\mu_{1,N} & -j\mu_{1,2} & \cdots & (j\omega_N - 1/\tau_o) \end{bmatrix} \begin{bmatrix} \hat{a}_1 \\ \hat{a}_2 \\ \vdots \\ \hat{a}_N \end{bmatrix} + \begin{bmatrix} -j\mu_i \hat{s}_i \\ 0 \\ \vdots \\ 0 \end{bmatrix} \quad (2.19)$$

In this expression  $1/\tau_i$  and  $1/\tau_o$  are the total rates of energy change in

microrings 1 and  $N$ , similar to  $1/\tau_c$  in equation (2.4). Assuming the signals to have harmonic time dependence, which allows us to write  $\hat{a}_k = a_k e^{j\omega t}$  and  $\hat{s}_i = s_i e^{j\omega t}$ , and defining the complex frequency variable  $s = j(\omega - \omega_o)$ , we can simplify (2.19) into the matrix equation

$$\left[ \left( s + \frac{1}{\tau_c} \right) \mathbf{I} + \mathbf{L} + j\mathbf{M} \right] \mathbf{a} = \mathbf{b}, \quad (2.20)$$

where  $\mathbf{a} = [a_1, a_2, \dots, a_N]^T$ ,  $\mathbf{b} = [-j\mu_i s_i, 0, \dots, 0]^T$ ,  $\mathbf{I}$  is the  $N \times N$  identity matrix,  $\mathbf{M}$  is an  $N \times N$  symmetric energy coupling matrix having the form

$$\mathbf{M} = \begin{bmatrix} \Delta\omega_1 & \mu_{1,2} & \cdots & \mu_{1,N} \\ \mu_{1,2} & \Delta\omega_2 & \cdots & \mu_{2,N} \\ \vdots & \vdots & \ddots & \vdots \\ \mu_{1,N} & \mu_{2,N} & \cdots & \Delta\omega_N \end{bmatrix}, \quad (2.21)$$

and  $\mathbf{L}$  is a diagonal matrix denoting the coupling between the input/output waveguides and the microring network as

$$\mathbf{L} = \text{diag}[\mu_i^2/2, 0, \dots, 0, \mu_o^2/2]. \quad (2.22)$$

Now obtaining the system response would simply mean solving equation (2.20). First, we factor the matrix  $-(\mathbf{L} + j\mathbf{M})$  into its eigenvalue decomposition as

$$-(\mathbf{L} + j\mathbf{M}) = \mathbf{Q} \cdot \mathbf{D} \cdot \mathbf{Q}^{-1}, \quad (2.23)$$

where  $\mathbf{D}$  is the diagonal matrix containing the eigenvalues, and  $\mathbf{Q}$  is the matrix containing the eigenvectors. Substitute (2.23) into (2.20), and we have

$$\mathbf{Q} \cdot \left[ \left( s + \frac{1}{\tau_c} \right) \mathbf{I} - \mathbf{D} \right] \cdot \mathbf{Q}^{-1} \mathbf{a} = \mathbf{b}. \quad (2.24)$$

The stored energies in the microring resonators are solved to give

$$\mathbf{a} = \mathbf{Q} \cdot \left[ \left( s + \frac{1}{\tau_c} \right) \mathbf{I} - \mathbf{D} \right]^{-1} \cdot \mathbf{Q}^{-1} \mathbf{b}. \quad (2.25)$$

Expanding the matrix product, we can write the expression for the amplitudes in each microring  $n$  as

$$a_n = -j\mu_i s_i \sum_{k=1}^N \frac{Q_{n,k} Q_{k,1}^{-1}}{s + 1/\tau_c - p_k}, \quad n = 1 \text{ to } N \quad (2.26)$$

where  $p_k$  is the  $k^{\text{th}}$  diagonal element of  $\mathbf{D}$ , or the  $k^{\text{th}}$  eigenvalue of  $-(\mathbf{L} + j\mathbf{M})$  in (2.23). Similar to equation (2.7), we can find the following relations at the input and output coupling junctions of microrings 1 and  $N$  as,

$$\begin{aligned} s_t &= s_i - j\mu_i a_1 \\ s_d &= -j\mu_o a_N \end{aligned} \quad (2.27)$$

Combining (2.26) and (2.27), we obtain the following closed form expressions for the transfer functions of the 2D CMR:

$$\frac{s_t}{s_i} = 1 - \mu_i^2 \sum_{k=1}^N \frac{Q_{1,k} Q_{k,1}^{-1}}{s + 1/\tau_c - p_k}, \quad (2.28)$$

$$\frac{s_d}{s_i} = -\mu_i \mu_o \sum_{k=1}^N \frac{Q_{N,k} Q_{k,1}^{-1}}{s + 1/\tau_c - p_k}. \quad (2.29)$$

In the above expressions, it can be seen that if the microrings are assumed to

be lossless ( $1/\tau_c = 0$ ), then the poles of the device transfer functions are given by  $p_k$ . Any loss in the microring would result in a shifting of the poles to the left in the  $s$ -plane. This property is useful in that it enables one to design lossy filters in which the effect of loss can be compensated by shifting the filter poles in the opposite direction through the pre-distortion technique [25]. In Chapter 3, it will be shown that we can derive similar expressions to equations (2.28) and (2.29) for strongly coupled CMRs using the field coupling formalism.

## 2.5 Summary

In this chapter, a theoretical overview of microring resonators is presented based on the energy coupling formalism. The transfer functions and spectral characteristics of single microring add/drop filters are derived. An energy coupling analysis of general 2D microring coupling topology is also presented. While the energy coupling formalism has been shown to be able to model various advanced coupled microring structures, its inherent assumption of weak coupling limits its applications to narrow-band filters. A more rigorous technique based on the field coupling formalism will be developed in the next chapter that can be used to analyze strongly coupled CMRs.

# Chapter 3

## Field Coupling Analysis of Coupled Microring Resonators

### 3.1 Field coupling formalism

In the field coupling formalism, each microring coupling junction is described by a coupled mode equation in space, whose solution leads to the coupling matrix description of the junction as in equation (2.1). The field coupling formalism is sometimes referred to as “coupling of modes in space” [26], and does not have the intrinsic assumption of uniform field distribution around the microring as in the energy coupling formalism. As a result it can more accurately describe a CMR structure under strong coupling. However, to date there is no systematic method to analyze CMRs using the field coupling formalism and the method has only been applied to analyze simple structures such as CROWs [27,28] and parallel-cascaded microring resonators [17,29]. In the followings, we develop a systematic approach which could be used to analyze general two dimensional CMR networks. This work has been published in [30] and [31].

We begin by considering a general coupled microring resonator network in

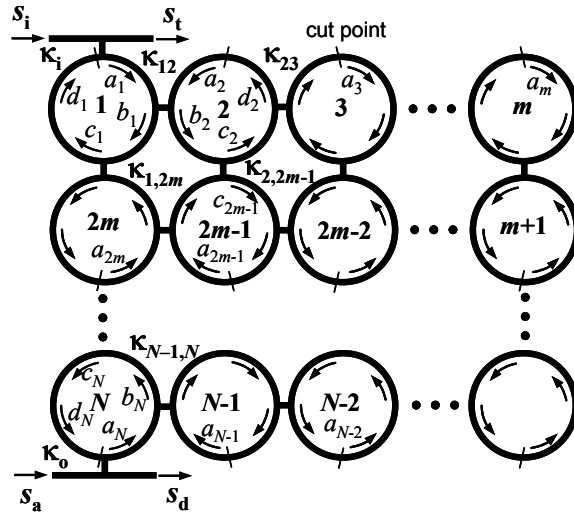


Figure 3.1. Schematic of a general 2D-CMR structure consisting of an  $n \times m$  array of  $N$  coupled microring resonators. [30]

the form of a two dimensional array of  $n \times m = N$  coupled microring resonators, as shown in Figure 3.1. This topology represents the most densely packed microring coupling configuration that does not give rise to coupling between counter-propagating waves in the microrings, which occurs in rhombic or hexagonal lattice due to the presence of triplets as shown in Figure 3.2. This restriction greatly simplifies the analysis, and does not give rise to a reflecting wave in the input bus, which is undesirable in many integrated optical filter applications. The microrings are labelled from 1 to  $N$  as shown in Figure 3.1, although the numbering does not affect the analysis. For simplicity, we also

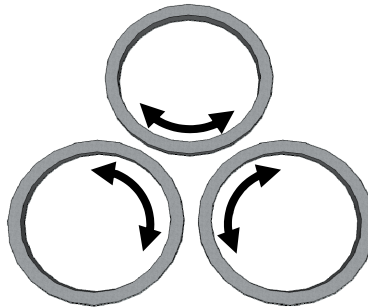


Figure 3.2 – Example of coupled microring triplets that would give rise to counter-propagation waves.

assume the microrings are identical with radius  $R$ , meaning they have the same resonant wavelengths, and all coupling junctions are lossless. A field coupling coefficient  $\kappa_{ij}$  describes the coupling between two adjacent microrings  $i$  and  $j$ . The input and output buses are also coupled to microrings 1 and  $N$ , respectively, via the input and output coupling coefficients  $\kappa_i$  and  $\kappa_o$ , respectively, as shown in the figure. The field amplitudes of the optical signals in the input and output buses are labelled as  $s_i$  (input),  $s_t$  (through),  $s_d$  (drop) and  $s_a$  (add). In each microring  $i$ , we follow the direction of the wave propagation and label the amplitude of the circulating wave in each quarter segment of the ring  $a_i, b_i, c_i, d_i$ , as shown in Figure 3.1. Note that we also maintain the order of labelling, i.e.  $a \rightarrow b \rightarrow c \rightarrow d$ , in different but adjacent microrings connected through coupling junctions. For example, in Figure 3.1, the field  $a_1$  in ring 1 is directly coupled to field  $b_2$  in ring 2 via coupling coefficient  $\kappa_{12}$ , which is then coupled to field  $c_{2m-1}$  in ring  $2m-1$  via coupling coefficient  $\kappa_{2,2m-1}$ , and so on. The reason for this labelling is that it will allow us to decompose the coupling matrix of the CMR structure into products of simpler matrices, which will become clear later.

To facilitate the analysis of the structure, we transform the two dimensional CMR network into an equivalent coupled-waveguide array as shown in Figure 3.3(a). The easiest way to visualize this process is to imagine “cutting” each microring at the point just before the field  $a_i$  is defined and unfolding the microring into a straight waveguide while keeping track of the coupling junctions between adjacent microrings and its coupling locations. Effectively, we have transformed the CMR structure in Figure 3.1 into its equivalent “unfolded”

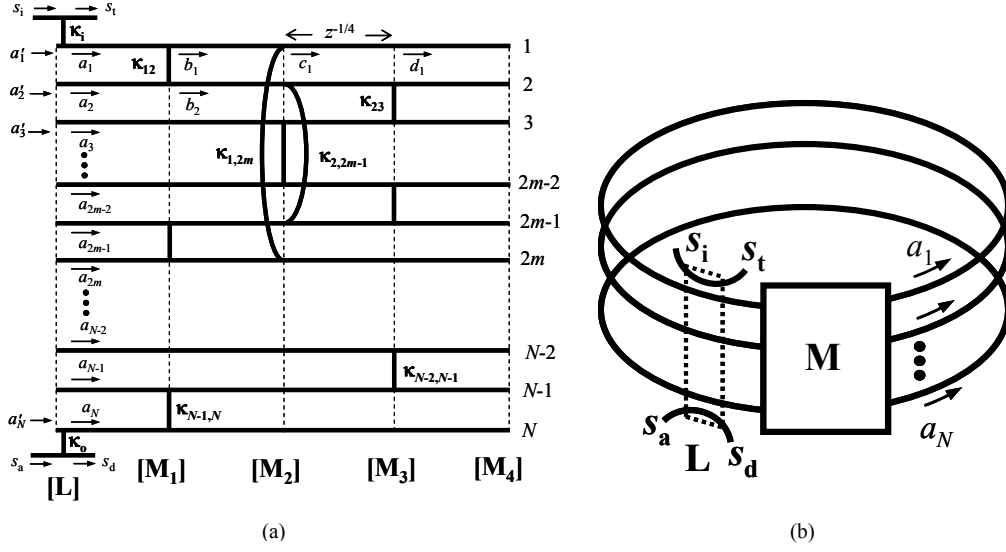


Figure 3.3. (a) Equivalent unfolded coupled-waveguide array of a general 2D-CMR. (b) “Stacked-rings” schematic of a 2D-CMR characterized by field coupling matrix  $\mathbf{M}$  and extrinsic loss matrix  $\mathbf{L}$ . [31]

configuration as shown in Figure 3.3(a), where each connection between the waveguides denotes coupling between two adjacent microrings. Also note that the resulting unfolded structure resembles an array of coupled Fabry-Perot waveguide cavities, except the reflective boundary conditions at the facets have been replaced with periodic boundary conditions, indicating that the waves can travel only in the forward direction (no counter propagating waves).

We now proceed to analyze the unfolded coupled-waveguide array using the transfer matrix method to determine the spectral response of the 2D-CMR structure. The coupled-waveguide array can be treated as four sections connected in series; each section representing a phase delay of a quarter ring,  $e^{-j\phi_{rt}/4} = z^{-1/4}$ , where  $\phi_{rt}$  is the microring roundtrip phase. The fields, or signals, in each section are denoted by arrays  $\mathbf{a}, \mathbf{b}, \mathbf{c}, \mathbf{d}$ , where

$$\mathbf{a} = [a_1, a_2, \dots, a_{N-1}, a_N]^T, \quad (3.1)$$



that within section  $k$ , it is always possible to renumber the waveguides so that the associated coupling matrix  $\mathbf{M}_k$  has the block-diagonal form similar to (3.2). This property is used in Section 3.6 – Appendix to prove that all the matrices  $\mathbf{M}_k$  are circular, i.e., they can be expressed in the form  $\mathbf{M}_k = \exp(j\mathbf{\Psi}_k)$ , where  $\mathbf{\Psi}_k$  is a real coupling-angle matrix [32].

We now apply transfer matrix analysis to the coupled-waveguide array. The field array in each section is related to the one following it by:

$$\mathbf{b} = z^{-1/4} \mathbf{M}_1 \mathbf{a}, \quad (3.5a)$$

$$\mathbf{c} = z^{-1/4} \mathbf{M}_2 \mathbf{b}, \quad (3.5b)$$

$$\mathbf{d} = z^{-1/4} \mathbf{M}_3 \mathbf{c}, \quad (3.5c)$$

$$\mathbf{a}' = z^{-1/4} \mathbf{M}_4 \mathbf{d}, \quad (3.5d)$$

$$\mathbf{a} = \mathbf{L} \mathbf{a}' + \mathbf{s}. \quad (3.5e)$$

In the above,  $\mathbf{s} = [-j\kappa_i s_i, 0, \dots, 0, -j\kappa_o s_o]^T$  is the input field array which contains all the input fields to the CMR structure;  $\mathbf{a}'$  is the field array defined just before the input and output bus coupling junctions (see Figure 3.3(a)), and  $\mathbf{L}$  is a diagonal matrix representing the bus-to-ring couplings,

$$\mathbf{L} = \text{diag}[\tau_i, 1, \dots, 1, \tau_o], \quad (3.6)$$

where  $\tau_{(i,o)} = \sqrt{1 - \kappa_{(i,o)}^2}$ . Combining the above equations we obtain

$$\mathbf{a}' = z^{-1} \mathbf{M}_4 \mathbf{M}_3 \mathbf{M}_2 \mathbf{M}_1 \mathbf{a} = z^{-1} \mathbf{M} \mathbf{a}, \quad (3.7)$$

where  $\mathbf{M}$  is the total ring-to-ring coupling matrix of the 2D-CMR and

$z^{-1} = e^{-j\phi_{\text{rt}}} = e^{-j\omega T_{\text{rt}}}$  is the roundtrip delay variable, with  $T_{\text{rt}} = 2\pi n_g R/c$  being the roundtrip time of the microrings with radius  $R$  and group index  $n_g$ . If there is loss in the microrings, it could be accounted for by defining  $z^{-1} = a_{\text{rt}} e^{-j\phi_{\text{rt}}}$ , where  $a_{\text{rt}}$  is the round-trip amplitude attenuation. Also, to account for small phase shifts in section  $k$  of the microrings, which may be intentionally introduced or arise due to fabrication or coupling-induced frequency shifts [33], the matrix  $\mathbf{M}_k$  is pre-multiplied by the factor  $\exp(j\mathbf{\Phi}_k)$ , where  $\mathbf{\Phi}_k = \text{diag}[\phi_1, \phi_2, \dots, \phi_N]$  represents the phase shifts in the waveguides. Substituting (3.7) into (3.5e) we obtain

$$(\mathbf{I} - z^{-1}\mathbf{LM})\mathbf{a} = \mathbf{s}, \quad (3.8)$$

where  $\mathbf{I}$  is the  $N \times N$  identity matrix. The above equation, which could be regarded as the characteristic equation of the 2D-CMR structure, shows that the spectral responses of the field amplitudes in a 2D-CMR are characterized by a field coupling matrix  $\mathbf{M}$ , which is determined by the coupling topology, and a ring-to-bus coupling matrix  $\mathbf{L}$  representing extrinsic loss due to coupling to the bus waveguides. Equation (3.8) also suggests that schematically, any 2D-CMR with arbitrary coupling topology may be represented by the “stacked-rings” block diagram as shown in Figure 3.3(b). It is also observed that the field-coupling equation in (3.8) has a somewhat similar form as the energy-coupling equation derived using the energy coupling in time formalism. (e.g., Equation (2.20)). The relationships between the parameters in the two formulations are derived in Section 3.4, where it is explicitly shown that Eq. (3.8) can be reduced to the energy coupling equation under the limit of weak coupling between the microring resonators.

It is also possible to obtain a closed form solution for the field array  $\mathbf{a}$  in the matrix equation (3.8). This is achieved by diagonalizing the matrix product  $\mathbf{LM} = \mathbf{QDQ}^{-1}$ , where  $\mathbf{D}$  is a diagonal matrix containing the eigenvalues of  $\mathbf{LM}$  and  $\mathbf{Q}$  is the corresponding eigenvector matrix. We then obtain from (3.8)

$$\mathbf{a} = \mathbf{Q}(\mathbf{I} - z^{-1}\mathbf{D})^{-1}\mathbf{Q}^{-1}\mathbf{s}. \quad (3.9)$$

If the input signal is applied only to the input port ( $s_i \neq 0, s_a = 0$ ), we can further simplify equation (3.9) and obtain the following expression for the field amplitude  $a_i$  in microring  $i$ ,

$$a_i = -j\kappa_i s_i \sum_{k=1}^N \frac{Q_{i,k} Q_{k,i}^{-1}}{1 - z^{-1}\lambda_k}, \quad (3.10)$$

where  $\lambda_k$  are the eigenvalues of  $\mathbf{LM}$  (diagonal elements of  $\mathbf{D}$ ) and  $Q_{i,k}$  and  $Q_{k,i}^{-1}$  are the elements of the matrices  $\mathbf{Q}$  and  $\mathbf{Q}^{-1}$ , respectively. The field amplitudes  $\mathbf{b}$ ,  $\mathbf{c}$  and  $\mathbf{d}$  in the microrings can be obtained from  $\mathbf{a}$  using (3.5a) – (3.5c).

### 3.1.1 Through-port and drop-port transfer functions

The transmission responses at the through port and drop port of the 2D-CMR network due to input signal  $s_i$  can be obtained by relating the output signals  $s_t$  and  $s_d$  to the field amplitudes  $a_1$  and  $a_N$  in microrings 1 and  $N$ . At the input bus-to-ring coupling junction of microring 1 (see Figure 3.3(a)), we have the relations

$$s_t = \tau_i s_i - j\kappa_i a'_1, \quad (3.11)$$

$$a_1 = -j\kappa_i s_i - \tau_i a'_1. \quad (3.12)$$

Eliminating  $a'_1$  from the above equations gives

$$s_t = \frac{1}{\tau_i} s_i - \frac{j\kappa_i}{\tau_i} a_1. \quad (3.13)$$

Using (3.10) for  $a_1$ , we get for the through-port response  $T_t$

$$T_t = \frac{s_t}{s_i} = \frac{1}{\tau_i} \left( 1 - \kappa_i^2 \sum_{k=1}^N \frac{Q_{1,k} Q_{k,1}^{-1}}{1 - z^{-1} \lambda_k} \right). \quad (3.14)$$

The above expression is also valid if the CMR structure is coupled to only one bus waveguide (i.e., the all-pass configuration). In this case the matrix  $\mathbf{L}$  in (3.6) has all ones on the diagonal except for the first element  $L_{11} = \tau_i$ .

For the drop port response, since we already assumed  $s_a = 0$ , we have the following relations at the output bus-to-ring coupling junction of microring  $N$ ,

$$s_d = -j\kappa_o a'_N, \quad (3.15)$$

$$a_N = \tau_o a'_N. \quad (3.16)$$

Combining the above equations and using (3.10), we obtain for the drop-port response

$$T_d = \frac{s_d}{s_i} = -\frac{j\kappa_o}{\tau_o} \frac{a_N}{s_i} = -\frac{\kappa_i \kappa_o}{\tau_o} \sum_{k=1}^N \frac{Q_{N,k} Q_{k,N}^{-1}}{1 - z^{-1} \lambda_k}. \quad (3.17)$$

Equations (3.14) and (3.17) give the closed form expressions for the through-port and drop-port transfer functions of a general 2D-CMR network and are one of the main results of the field coupling analysis. If we take the squared modulus of each term in the summation of (3.17), we obtain an expression of the form

$$\left| \frac{\mathcal{Q}_{N,k} \mathcal{Q}_{k,N}^{-1}}{1 - \lambda_k e^{-j\phi_n}} \right|^2 \propto \frac{I_k}{1 + F_k \sin^2(\phi_n)}, \quad (3.18)$$

which has the form of an Airy function. Thus the response of a 2D-CMR consists of a sum of  $N$  Airy resonances. This is an intuitive result but has not been proved for a general 2D-CMR structure before. In the limit of weak coupling, the device response reduces to a sum of  $N$  Lorentzian resonances, a result which can be obtained by taking the square modulus of each term of equations (2.28) and (2.29).

Note that the transfer functions of the 2D-CMR (3.14) and (3.17) have the form of rational functions of the roundtrip delay variable  $z^{-1}$ ,

$$T_t(z^{-1}) = \frac{R(z^{-1})}{Q(z^{-1})}, \quad (3.19a)$$

$$T_d(z^{-1}) = \frac{P(z^{-1})}{Q(z^{-1})}. \quad (3.19b)$$

In the above  $R(z^{-1})$  and  $Q(z^{-1})$  are polynomials of degree  $N$ , which corresponds to the order, or number of microrings in the network. The roots of  $Q(z^{-1})$  are the  $N$  resonances or poles of the device, which in the absence of resonator loss are given by the inverse of the eigenvalues,  $1/\lambda_k$ , of the matrix product  $\mathbf{LM}$ . For the polynomial  $P(z^{-1})$ , the coefficient of its highest-power term, the  $(N-1)^{\text{th}}$  power, is given by

$$p_{N-1} = -\frac{\kappa_i \kappa_o}{\tau_o} \sum_{k=1}^N \mathcal{Q}_{N,k} \mathcal{Q}_{k,1}^{-1}, \quad (3.20)$$

which is zero since the summation is the product of row  $N$  of  $\mathbf{Q}$  and column 1 of

$\mathbf{Q}^{-1}$ . Thus  $P(z^{-1})$  has a maximum degree of only  $N - 2$ , yielding a maximum of  $N - 2$  transmission zeros for the drop-port transfer function. Similar expressions are also obtained for weakly-coupled 2D-CMR structures using the energy coupling formalism, where the drop-port and through-port transfer functions are rational functions of the frequency parameter  $s = j\omega$  as seen in (2.28) and (2.29).

### 3.1.2 2D-CMRs with no external bus waveguides

Coupled microring resonators with no external bus waveguides are sometimes referred to as “photonic molecules” since they exhibit photon states similar to electronic states of a molecule [34]. These structures have potential applications such as microlasers [35], quantum emulators and simulators [36]. Tight binding analysis has been applied to determine the quantum states of simple coupled cavity systems such as a twin disk [37], but this approach is strictly valid only for weakly coupled systems. For strongly-coupled photonic molecules, the supermodes of the structure would have non-uniform field distribution within each microring, so that an accurate determination of the eigenstates and eigenvalues of the structure requires a field coupling analysis. In an isolated 2D-CMR with no external bus waveguides ( $\kappa_i = \kappa_o = 0$ ,  $s = 0$ ), the bus-to-ring coupling matrix  $\mathbf{L} = \mathbf{I}$  and (3.8) becomes an eigenvalue equation

$$(\mathbf{I} - z^{-1}\mathbf{M})\mathbf{a} = 0. \quad (3.21)$$

Solutions of  $\mathbf{a}$  in the above equation are the  $N$  orthogonal eigenvectors  $\mathbf{Q}$  of the coupling matrix  $\mathbf{M}$ . Along with the associated solutions for the field arrays  $\mathbf{b}$ ,  $\mathbf{c}$  and  $\mathbf{d}$  in the microrings, they constitute the  $N$  supermodes of the photonic molecule. The resonance frequency  $\omega_k$  (or energy level  $\hbar\omega_k$ ) of the supermode  $k$

is given by  $\omega_k = -\phi_k/T_{\text{rt}}$ , where  $\phi_k = \angle\lambda_k$  is the phase of the  $k^{\text{th}}$  eigenvalue of the coupling matrix  $\mathbf{M}$  and  $T_{\text{rt}}$  is the roundtrip time of the microrings.

### 3.1.3 Direct and indirect coupling-angle matrices

In the energy coupling formulation of weakly-coupled microring resonator networks, a 2D-CMR is characterized by an energy-coupling matrix which describes the direct couplings between the microring resonators (Equation (2.21)). In this section we show that in the field coupling formulation, the field coupling matrix  $\mathbf{M}$  in (3.8) can be decomposed into a sum of a direct coupling-angle matrix plus a term representing all indirect resonator couplings. In this case, the indirect coupling refers to the effective coupling which arises from all indirect coupling pathways between two microrings, which could also include those that exist between two adjacent resonators. We will later show by example that the indirect coupling matrix can give rise to distinct resonance features not observed in weakly-coupled CMRs.

In Section 3.6 – Appendix, it is shown that the matrix  $\mathbf{M}_k$  of each section  $k$  of the coupled-waveguide array is circular, which means it can be expressed as

$$\mathbf{M}_k = \mathbf{W}_k \mathbf{\Lambda}_k \mathbf{W}_k^T = e^{j\mathbf{W}_k}, \quad (3.22)$$

where  $\mathbf{\Lambda}_k$  is a diagonal matrix containing the eigenvalues of  $\mathbf{M}_k$  and  $\mathbf{W}_k$  is the corresponding (real) eigenvector matrix. The eigenvalues of  $\mathbf{M}_k$  are given by

$$\mathbf{\Lambda}_k(i,i) = \mathbf{\Lambda}_k(j,j) = \tau_{i,j} - j\kappa_{i,j} = e^{j\theta_{i,j}}, \quad (3.23)$$

where  $\theta_{i,j} = -\tan^{-1}(\kappa_{i,j}/\tau_{i,j})$  is the coupling angle between waveguides  $i$  and  $j$ .

If waveguide  $i$  of section  $k$  is not coupled to any other waveguide then we simply have  $\Lambda_k(i, i) = 1$ . The matrix  $\Psi_k$  in (3.22) is the coupling-angle matrix for section  $k$  of the coupled-waveguide array (see Equations (3.47) and (3.48) in Section 3.6 ), and it is real and symmetric with zero diagonal elements. The off-diagonal elements are also zero except if there is direct coupling between waveguides  $i$  and  $j$ , then  $\Psi_k(i, j) = \Psi_k(j, i) = \theta_{i,j}$ . Using (3.22), the total coupling matrix  $\mathbf{M}$  of the 2D-CMR can be expressed as

$$\mathbf{M} = \mathbf{M}_4 \mathbf{M}_3 \mathbf{M}_2 \mathbf{M}_1 = e^{j\Psi_4} e^{j\Psi_3} e^{j\Psi_2} e^{j\Psi_1}. \quad (3.24)$$

Since the matrices  $\mathbf{M}_k$  do not commute in general, we expand the product of the matrix exponentials in (3.24) using the Baker-Campbell-Hausdorff formula [38] as

$$\mathbf{M} = \exp\left(\sum_{k=1}^4 j\Psi_k + j\mathbf{X}\right) = \exp(j\Psi + j\mathbf{X}). \quad (3.25)$$

In the above, the matrix sum  $\Psi = \Psi_1 + \Psi_2 + \Psi_3 + \Psi_4$  is a symmetric matrix with zero's on the diagonal and off-diagonal elements  $\Psi(i, j) = \Psi(j, i)$  given by the coupling angle  $\theta_{i,j}$  between microrings  $i$  and  $j$ . The matrix  $\mathbf{X}$  denotes the sum of all nested commutators,

$$\mathbf{X} = \sum_m^{\infty} P_m(\Psi_1, \Psi_2, \Psi_3, \Psi_4), \quad (3.26)$$

where  $P_m$  represents polynomials of the commutators of the matrices  $\Psi_k$ . Equation (3.25) shows that in general a 2D-CMR structure is characterized by a

coupling-angle matrix  $\Psi$  plus a commutation matrix  $\mathbf{X}$ . The matrix  $\Psi$  accounts for the direct couplings between adjacent microring resonators and has the same form as the energy coupling matrix  $\mathbf{M}$  in equation (2.21) in the energy coupling formulation, except that its  $(i, j)$  element is given by the coupling angle  $\theta_{i,j}$  instead of the energy coupling coefficient  $\mu_{i,j}$ . The significance of the direct coupling-angle matrix  $\Psi$  is that it explicitly shows the coupling topology of the 2D-CMR structure, i.e., the topology of the device can be reconstructed and the values of the coupling elements determined if  $\Psi$  is known. By contrast, it is not possible to reconstruct the CMR topology based on the field coupling matrix  $\mathbf{M}$ , which is in general a full and complex-valued matrix.

The commutation matrix  $\mathbf{X}$  in (3.24) accounts for the effective couplings arising from all the indirect coupling paths between two microrings. It is in general a full but symmetric matrix, with alternating diagonal bands of real and pure imaginary elements. In the limit of weak coupling, the indirect coupling term can be neglected ( $\mathbf{X} \approx 0$ ) so that the coupling matrix  $\mathbf{M}$  can be approximated by only the direct coupling term,  $\mathbf{M} \approx \exp(j\Psi)$ . This is indeed the approximation made in the energy coupling formulation of 2D-CMRs, as will be shown in Section 3.4. It can thus be said that the energy coupling formulation does not take into account the effect of the indirect couplings.

For certain microring coupling topologies for which the matrices  $\mathbf{M}_k$  in (3.24) do commute, the commutation term also vanishes. One such special case is a quadruplet, with identical coupling coefficients  $\kappa_{i,j} = \kappa$ , arranged in a  $2 \times 2$  square which can be seen in Figure 3.4(a) whose field coupling matrices are included in

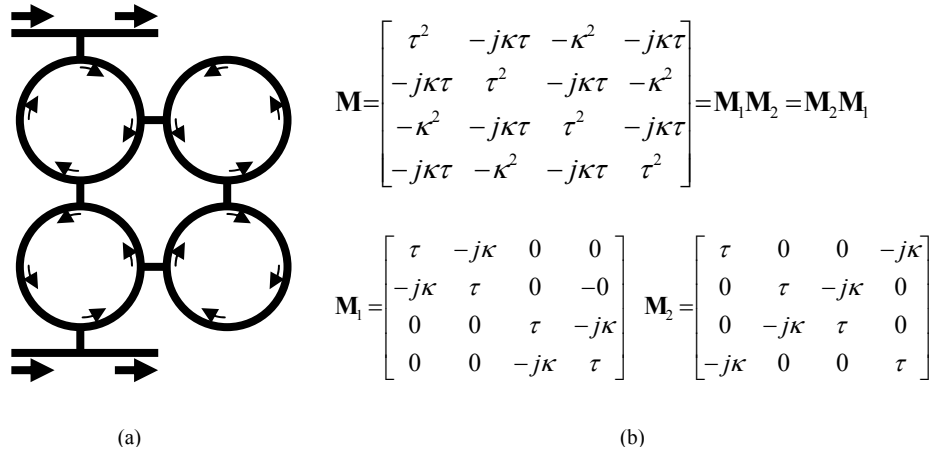


Figure 3.4 – Special case of a quadruplet CMR network arranged in 2x2 square (a), and its corresponding field coupling matrices (b)

Figure 3.4(b). For this structure it can be shown that  $\mathbf{M}_3 = \mathbf{M}_4 = \mathbf{I}$  and  $\mathbf{M}_1$  and  $\mathbf{M}_2$  commute with each other so that  $\mathbf{X} = 0$ . All the indirect coupling paths cancel themselves out and the coupling matrix is given by only the direct couplings between adjacent resonators,  $\mathbf{M} = \exp(j\Psi)$ .

### 3.2 Example of a 3x3 2D-CMR

To demonstrate the effect of the indirect coupling term on the 2D-CMR's spectral response, we consider a 3x3 2D-CMR structure as shown in Figure 3.5(a) under both weak and strong coupling conditions. The coupling coefficients are chosen to be  $\kappa_i = \kappa_o = 0.2$  (couplings to the input and output buses),  $\kappa_{25} = \kappa_{45} = \kappa_{56} = \kappa_{58} = \kappa_1$  (couplings to the center microring) and all the remaining coupling coefficients  $\kappa_{i,j} = \kappa_2$ . For the weak coupling case, we let  $\kappa_1 = 0.02$  and  $\kappa_2 = 0.015$  whereas for the strong coupling case  $\kappa_1 = 0.2$  and  $\kappa_2 = 0.15$ . The unfolded coupled-waveguide array is shown in Figure 3.5(b).

To visualize the effect of indirect coupling, we plot the magnitude of the direct and indirect coupling matrices  $\Psi$  and  $\mathbf{X}$  of the strongly-coupled device in

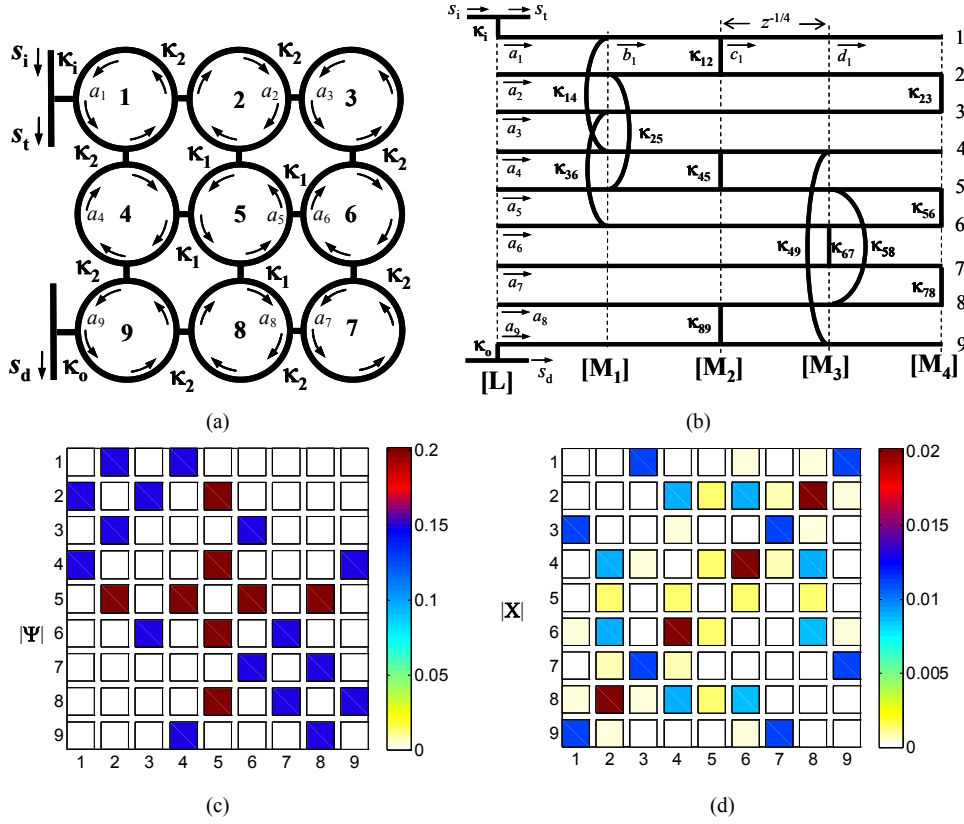


Figure 3.5. (a) 3x3 2D-CMR structure. (b) Unfolded coupled-waveguide array. (c) and (d) Magnitudes of the elements of the direct and indirect coupling matrices of the strongly-coupled CMR structure. [31]

Figures 3.5(c) and (d). The elements of the direct coupling matrix  $\Psi$  is non-zero only if there is a direct coupling between the two adjacent microrings as shown in the unfolded waveguide array. However, matrix  $\mathbf{X}$  shows that in general there could be nonzero elements which indicate indirect couplings between both adjacent and non-adjacent microrings.

We compare the drop-port spectral response of the 2D-CMR structure under weak and strong coupling conditions in Figures 3.6(a) and 3.5(b). For the weakly-coupled case, its spectral response (solid black line in Figure 3.6(a)) shows two resonance peaks at the normalized frequencies  $\Delta f/FSR = \pm 0.05$  and three transmission nulls. For the strongly coupled case (Figure 3.6(b)), we

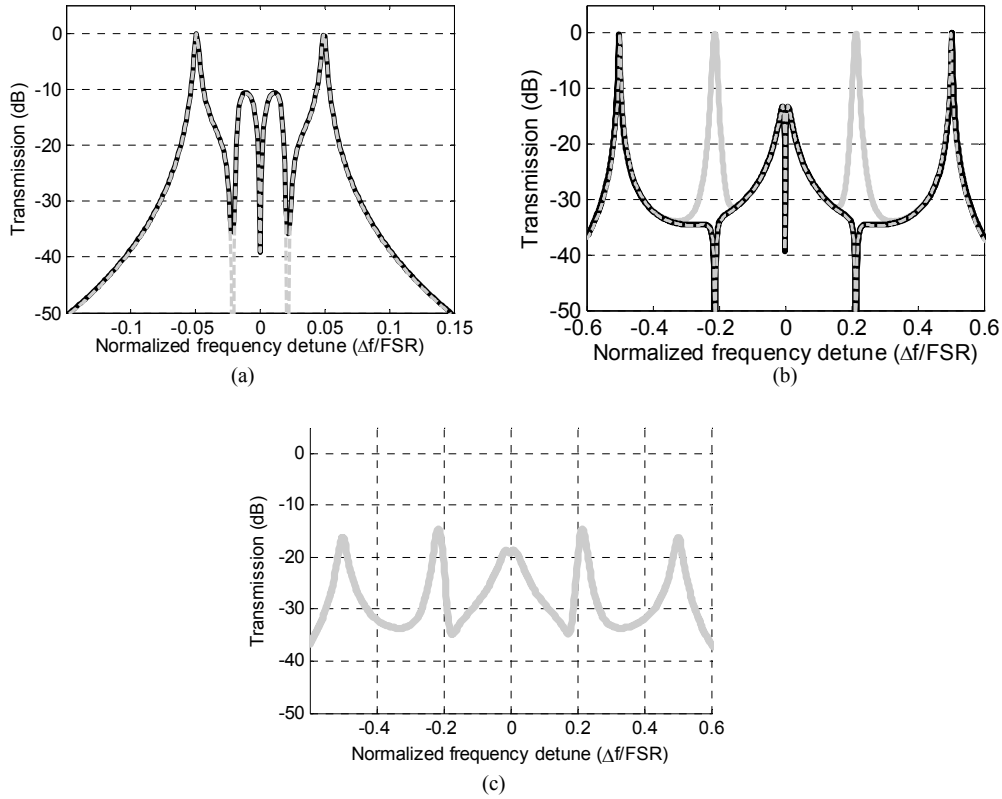


Figure 3.6. Drop-port response of the  $3 \times 3$  2D-CMR under (a) weak coupling and (b) strong coupling conditions. In (a), results were computed using field coupling (solid black line) and energy coupling (dashed grey line). In (b), results were computed using field coupling with (solid grey line) and without (solid black line) indirect coupling matrix  $\mathbf{X}$ . Energy coupling result is shown by dashed grey line. [31] In (c) drop port response in the strong coupling case is calculated using field coupling with 1% round-trip loss

plotted the device response computed with the indirect coupling matrix  $\mathbf{X}$  neglected (i.e.,  $\mathbf{M} = \exp(j\Psi)$ , black solid line) and as well with matrix  $\mathbf{X}$  included (i.e.,  $\mathbf{M} = \exp(j\Psi + j\mathbf{X})$ , grey solid line).

It could be seen that with the indirect coupling term neglected, the device's spectral response is similar to that of the weakly-coupled device (Figure 3.6(a)), with two resonance peaks and three transmission nulls. However, when the indirect coupling term is included, the device exhibits two additional resonance peaks at the frequencies  $\pm 0.2$ , where the transmission nulls were located in the case where we ignored indirect coupling. This shows that the new resonance

peaks are caused by the indirect coupling term ( $\mathbf{X}$ ). In analogy to the phenomenon of coupled-resonator-induced transparency (CRIT) [4], we may refer to this effect as “indirect coupling induced transparency” to emphasize the origin of the observed transmission peaks.

For comparison, we also plotted in Figures 3.6(a) and (b) the device responses obtained using the energy coupling formalism (dashed grey lines). For the weakly-coupled device, the energy coupling analysis yields almost identical device responses to the field coupling analysis. However, in the strongly coupled device, the energy coupling result is in agreement with the field coupling result only when we have neglected the indirect coupling term. We can also show that these discrepancies in the analyzed spectral responses are not related to loss. The drop port spectral response of the same strongly coupled structure with 1% round-trip loss (i.e. round-trip amplitude transmission of 99%, or  $z^{-1} = 0.99e^{-j\phi_n}$ ) is plotted in Figure 3.6(c), where resonance peaks are also observed at frequencies  $\pm 0.2$ , similar to the full field coupling result in Figure 3.6(b).

To further understand the reason behind the appearance of the new transmission peaks under the strong coupling case, we have plotted the pole-zero diagrams for the drop port response as shown in Figure 3.7. In the case where  $\mathbf{X}$  is neglected (Figure 3.7(a)), the resonances (in the form of double poles) at the frequencies  $\pm 0.2$  are seen to be suppressed by the presence of two zeros occurring at the same locations. However, if we use the full field coupling matrix with  $\mathbf{X}$  included (Figure 3.7(b)), the two zeros at  $\pm 0.2$  begin to split and move away from

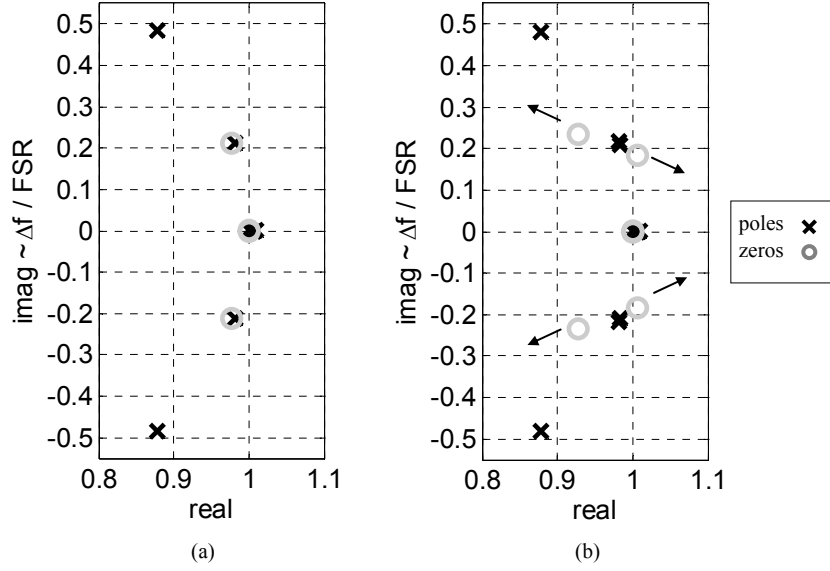


Figure 3.7. Pole-zero diagram of the 3×3 2D-CMR under strong coupling condition computed (a) without and (b) with the indirect coupling matrix  $\mathbf{X}$ . [31]

the suppressed poles, thereby giving rise to the new transmission peaks. This example illustrates that indirect resonator couplings can indeed have a pronounced effect on the device response and should not be neglected in the design and analysis of strongly-coupled 2D-CMRs. Since the energy coupling formalism has been shown to ignore the indirect coupling term, it is not appropriate for the analysis and design of strongly-coupled microring resonators with broad transmission bandwidths.

### 3.3 Similarity transformations of the field coupling matrix

Similarity transformations have been exploited in the energy coupling formalism to simplify and optimize weakly-coupled 2D-CMRs in order to achieve better coupling topologies [5]. In this section, we show that it is also possible to apply such similarity transformations on the coupling-angle matrix of strongly-coupled 2D-CMRs without altering the device’s spectral characteristics.

Let  $\mathbf{R}$  represent an  $N \times N$  similarity transformation matrix that does not disturb the first or last row of a vector/matrix. The latter assumption is necessary so that the transformation does not alter the coupled input and output bus signals. Applying  $\mathbf{R}$  to both sides of (3.8) and using the fact that  $\mathbf{R}\mathbf{R}^T = \mathbf{I}$ , we can write

$$\mathbf{R}(\mathbf{I} - z^{-1}\mathbf{L}\mathbf{M})\mathbf{R}^T \mathbf{R}\mathbf{a} = \mathbf{R}\mathbf{s}. \quad (3.27)$$

Since  $\mathbf{s}$  and  $\mathbf{L}$  are nonzero only in the first and last element/row, the transformation does not disturb them so we have  $\mathbf{R}\mathbf{s} = \mathbf{s}$  and  $\mathbf{R}\mathbf{L} = \mathbf{L}\mathbf{R}$ . The above equation can thus be simplified as

$$(\mathbf{I} - z^{-1}\mathbf{L}\mathbf{M}')\mathbf{a}' = \mathbf{s} \quad (3.28)$$

where  $\mathbf{M}' = \mathbf{R}\mathbf{M}\mathbf{R}^T$  is the new field coupling matrix and  $\mathbf{a}' = \mathbf{R}\mathbf{a}$  is the new field arrays. Writing  $\mathbf{M} = \exp(j\mathbf{\Psi} + j\mathbf{X})$ , we can express  $\mathbf{M}'$  as

$$\mathbf{M}' = \mathbf{R} \exp(j\mathbf{\Psi} + j\mathbf{X})\mathbf{R}^T = \exp(j\mathbf{\Psi}' + j\mathbf{X}'), \quad (3.29)$$

where  $\mathbf{\Psi}' = \mathbf{R}\mathbf{\Psi}\mathbf{R}^T$  and  $\mathbf{X}' = \mathbf{R}\mathbf{X}\mathbf{R}^T$ . This result shows that applying a similarity transformation  $\mathbf{R}$  to the field coupling matrix  $\mathbf{M}$  is equivalent to applying the same transformation simultaneously to both the direct ( $\mathbf{\Psi}$ ) and the indirect ( $\mathbf{X}$ ) coupling matrices. Thus in applying similarity transformations to optimize or generate new coupling topologies, we can perform the optimization directly on  $\mathbf{\Psi}$  (and simultaneously on  $\mathbf{X}$ ) instead of  $\mathbf{M}$ . This is an important observation since as mentioned earlier, the coupling topology (and its coupling values) of a CMR structure can be determined from the direct coupling-angle matrix  $\mathbf{\Psi}$ , but not from the total field coupling matrix  $\mathbf{M}$ .

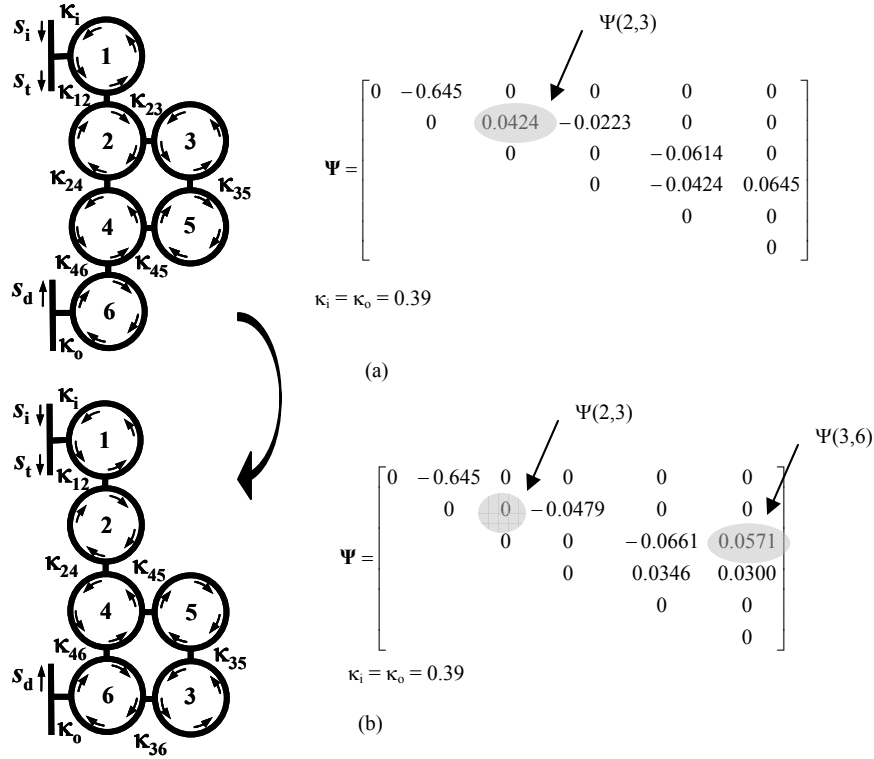


Figure 3.8. Generation of a new microring coupling topology by similarity transformation of the coupling-angle matrix: (a) original coupling topology; (b) transformed coupling topology. The direct coupling-angle matrix  $\Psi$  of each topology is also shown. [31]

To illustrate the application of similarity transformations to generate new microring coupling topologies, we consider the 2D-CMR structure consisting of 6 microrings with coupling topology shown in Figure 3.8(a). Its direct coupling-angle matrix is also shown on the right. The values of the coupling angles were obtained from the design of an inverse Chebyshev filter using the energy-coupling method presented in [5]. An alternative coupling topology of the device can be generated by eliminating the coupling between microrings 2 and 3. This can be accomplished by applying a Jacobi rotation matrix  $\mathbf{R}$  given by

$$\mathbf{R} = \begin{bmatrix} 1 & & & & & \\ & 1 & & & & \\ & & \cos\theta & \sin\theta & & \\ & & -\sin\theta & \cos\theta & & \\ & & & & 1 & \\ & & & & & 1 \end{bmatrix}, \quad (3.30)$$

with the rotation angle  $\theta$  chosen such that the element (2, 3) of the new direct coupling matrix  $\Psi' = \mathbf{R}\Psi\mathbf{R}^T$  is zero. By multiplying out the product  $\mathbf{R}\Psi\mathbf{R}^T$ , we can show that the element (2, 3) of matrix  $\Psi'$  could be annihilated if the rotation angle  $\theta = \tan^{-1}[\Psi(2, 3)/\Psi(2, 4)] = -1.0869$ . The new direct coupling matrix  $\Psi$  and the associated coupling topology are shown in Figure 3.8(b). It is seen that the annihilation of the coupling between microrings 2 and 3 in the old topology in this case generates a new coupling between microrings 3 and 6. Note that this operation has not only changed the device's coupling topology, but also the values of some of the coupling angles as well. The devices' spectral responses are

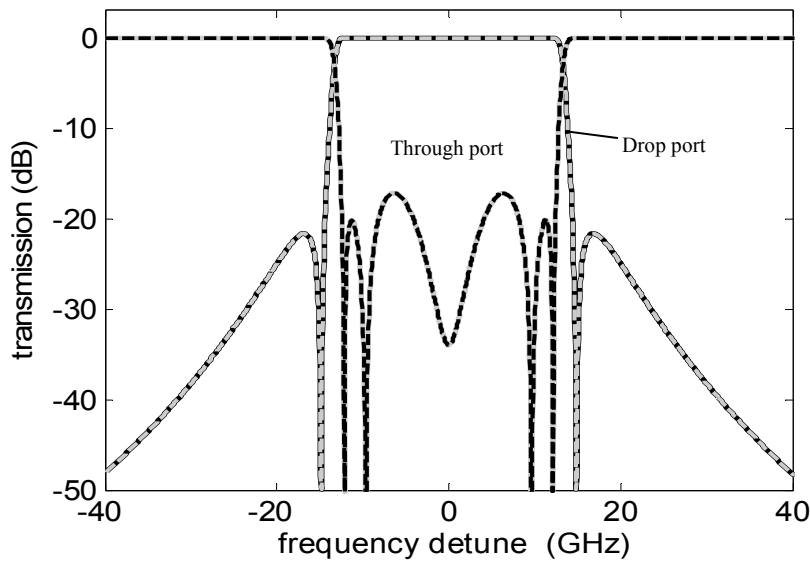


Figure 3.9. Drop-port and through-port spectral responses of the CMR structure in Figure 6(a) (solid lines) and Figure 6(b) (dashed lines). [31]

plotted in Figure 3.9, which confirms that the two CMR topologies indeed have identical drop-port and through-port spectral responses. In general, similarity transformations can also be used to optimize a CMR structure by eliminating as many coupling elements as possible in the coupling topology, as typically done in the coupling matrix synthesis of CMR filters [5, 39].

### 3.4 Relationship between energy and field coupling formulations

In this section, we show that the characteristic equation of a 2D-CMR in the energy coupling formulation, Equation (2.20), can be directly derived from the field coupling formalism (Equation (3.8)) under the weak coupling and narrowband approximations. Explicit relationships between the parameters in both formulations will also be derived.

First, we note that since the bus-to-ring coupling matrix  $\mathbf{L}$  in (3.6) is diagonal, we can express it as  $\mathbf{L} = \exp(\mathbf{A})$ , where

$$\mathbf{A} = \text{diag}[\ln(\tau_i), 0, \dots, 0, \ln(\tau_o)]. \quad (3.31)$$

If we assume the input and output bus couplings are weak ( $\tau_i \approx 1$  and  $\tau_o \approx 1$ ), then  $\mathbf{L} \approx \mathbf{I}$ , so that  $\mathbf{LM} \approx \mathbf{ML}$ , i.e.,  $\mathbf{L}$  and  $\mathbf{M}$  commute. This approximation allows us to write (3.8), with the help of (3.25) and (3.31), as

$$[\mathbf{I} - z^{-1} \exp(\mathbf{A} + j\mathbf{\Psi} + j\mathbf{X})]\mathbf{a} = \mathbf{s}. \quad (3.32)$$

For the roundtrip delay variable  $z^{-1}$ , we have

$$z^{-1} = a_{rt} e^{-j\phi_{rt}} = e^{-(\gamma + j\omega)T_{rt}}, \quad (3.33)$$

where  $\gamma = 1/\tau_c = -\ln(a_{rt})/T_{rt}$  is the rate of energy loss from each resonator,  $\tau$  is the

intrinsic cavity lifetime, and  $T_{\text{rt}}$  is the roundtrip time of the microrings. Substituting (3.33) into (3.32) gives

$$\{\mathbf{I} - \exp[-(\gamma + j\omega)T_{\text{rt}}\mathbf{I} + \mathbf{A} + j\mathbf{\Psi} + j\mathbf{X}]\}\mathbf{a} = \mathbf{s}. \quad (3.34)$$

Now we apply the narrowband approximation by assuming that the argument of the exponential in (3.34) is small over a narrow frequency range around the microring resonance of interest. This allows us to expand the exponential to the first order as

$$\begin{aligned} \exp[-(\gamma + j\omega)T_{\text{rt}}\mathbf{I} + \mathbf{A} + j\mathbf{\Psi} + j\mathbf{X}] \approx \\ \mathbf{I} - (\gamma + j\omega)T_{\text{rt}}\mathbf{I} + \mathbf{A} + j\mathbf{\Psi} + j\mathbf{X} \end{aligned} \quad (3.35)$$

which, after substitution into (3.34), gives

$$[(\gamma + j\omega)T_{\text{rt}}\mathbf{I} - \mathbf{A} - j\mathbf{\Psi} - j\mathbf{X}]\mathbf{a} = \mathbf{s} \quad (3.36)$$

or

$$\left[ (s + \gamma)\mathbf{I} - \frac{1}{T_{\text{rt}}}(\mathbf{A} + j\mathbf{\Psi} + j\mathbf{X}) \right] (T_{\text{rt}}\mathbf{a}) = \mathbf{s}, \quad (3.37)$$

where  $s = j\omega$  is the complex frequency variable. Under weak coupling condition, we could assume the field amplitude in each microring is approximately uniform (i.e.,  $\mathbf{a} \approx \mathbf{b} \approx \mathbf{c} \approx \mathbf{d}$ ), in which case the term  $T_{\text{rt}}\mathbf{a} = \hat{\mathbf{a}}$  can be regarded as representing the amplitudes of the energies stored in the microrings. We further define the relationships

$$\mathbf{\Gamma} = -\frac{1}{T_{\text{rt}}}\mathbf{A} \approx \frac{1}{2T_{\text{rt}}}\text{diag}[\kappa_1^2 \quad 0 \quad \dots \quad 0 \quad \kappa_0^2], \quad (3.38)$$

$$\mathbf{\mu} = -\frac{1}{T_{\text{rt}}}\mathbf{\Psi}, \quad (3.39)$$

where the elements of  $\boldsymbol{\mu}$  are given by

$$\mu_{i,j} = -\frac{1}{T_{\text{rt}}} \boldsymbol{\Psi}(i, j) = \frac{1}{T_{\text{rt}}} \tan\left(\frac{\kappa_{i,j}}{\tau_{i,j}}\right) \approx \frac{\kappa_{i,j}}{T_{\text{rt}}}. \quad (3.40)$$

In the above  $\boldsymbol{\Gamma}$  gives the rates of energy coupling between the external bus waveguides and the CMR network, and  $\boldsymbol{\mu}$  is the direct energy coupling matrix whose element  $\mu_{i,j}$  gives the rate of energy transfer between microrings  $i$  and  $j$ . Using (3.38) and (3.39) in (3.37) and neglecting the indirect coupling matrix  $\boldsymbol{X}$ , we obtain the energy coupling equation for a weakly-coupled CMR,

$$((s + \gamma)\mathbf{I} + \boldsymbol{\Gamma} + j\boldsymbol{\mu})\hat{\boldsymbol{a}} = \hat{\boldsymbol{s}}, \quad (3.41)$$

where  $\hat{\boldsymbol{s}} = [\hat{s}_i, 0, 0, \dots, \hat{s}_a]$  represents the rates of external energies being applied to the input and add ports of the device. Equation (3.41) is the same as (2.20), where  $\boldsymbol{\Gamma}=\mathbf{L}$ ,  $\boldsymbol{\mu}=\mathbf{M}$ , and  $\gamma=1/\tau_c$ .

### 3.5 Summary

In this chapter, we presented an analytic theory for analyzing general two dimensional coupled microring resonator networks based on the field coupling formalism. It was shown that the field coupling matrix can be decomposed into a direct and indirect coupling term. The indirect coupling term is neglected in the energy coupling formulation but could have prominent contributions to the device's spectral characteristics under strong coupling between the microring resonators. We also showed how the energy formulation of 2D-CMR networks can be derived from the field coupling formulation under the weak coupling and narrow band approximations. Finally we showed that similarity transformations

can also be applied to the field coupling matrix in the field coupling formalism to generate new CMR coupling topologies having the same spectral characteristics.

### 3.6 Appendix – Proof of the Circular Property of the Field Coupling Matrices

We show in this section that the coupling matrix  $\mathbf{M}_k$  associated with each section  $k$  of the coupled-waveguide array in Figure 3.3(a) is circular. First we note that each  $2 \times 2$  coupling matrix  $\mathbf{K}_{i,j}$  in the block-diagonal matrix  $\mathbf{M}_1$  in (3.2) has the eigenvalue decomposition

$$\mathbf{K}_{i,j} = \mathbf{W} e^{j\Theta_{i,j}} \mathbf{W}^T, \quad (3.42)$$

where  $\Theta_{i,j} = \text{diag}[\theta_{i,j}, -\theta_{i,j}]$ ,  $\theta_{i,j} = -\tan^{-1}(\kappa_{i,j} / \tau_{i,j})$  is the coupling angle between microrings  $i$  and  $j$ , and the eigenvector matrix is

$$\mathbf{W} = \frac{1}{\sqrt{2}} \begin{bmatrix} 1 & 1 \\ 1 & -1 \end{bmatrix}. \quad (3.43)$$

It follows that  $\mathbf{K}_{i,j}$  is a circular matrix since it can be expressed as

$$\mathbf{K}_{i,j} = e^{j\mathbf{W}\Theta_{i,j}\mathbf{W}^T} = e^{j\Psi_{i,j}}, \quad (3.44)$$

where  $\Psi_{i,j}$  is a real coupling-angle matrix given by

$$\Psi_{i,j} = \mathbf{W}\Theta_{i,j}\mathbf{W}^T = \begin{bmatrix} 0 & \theta_{i,j} \\ \theta_{i,j} & 0 \end{bmatrix}. \quad (3.45)$$

Since the block-diagonal matrix  $\mathbf{M}_1$  is composed of either the matrices  $\mathbf{K}_{i,j}$  or 1's on its diagonal, it can be diagonalized in the form

$$\mathbf{M}_1 = \mathbf{W}_1 e^{j\Theta_1} \mathbf{W}_1^T = e^{j\Psi_1}, \quad (3.46)$$

where  $\Theta_1$  is a diagonal matrix containing the coupling angles associated with the coupling junctions of  $\mathbf{M}_1$  and  $\mathbf{W}_1$  is the corresponding (real) eigenvector matrix. The matrix  $\Psi_1 = \mathbf{W}_1 \Theta_1 \mathbf{W}_1^T$  is the direct coupling-angle matrix of section 1, with the property that all its elements are zero except for  $\Psi_1(i, j) = \theta_{i,j}$  if there is coupling between waveguides  $i$  and  $j$ . Equation (3.46) indicates that  $\mathbf{M}_1$  is a circular matrix. According to (3.4)  $\mathbf{M}_2$ ,  $\mathbf{M}_3$  and  $\mathbf{M}_4$  can be converted to the block diagonal form as  $\mathbf{M}_1$  via a suitable permutation matrix  $\mathbf{P}_k$ . It follows then that these matrices are also circular since they can be expressed as

$$\mathbf{M}_k = \mathbf{P}_k (\mathbf{W}_1 e^{j\Theta_1} \mathbf{W}_1^T) \mathbf{P}_k^T = e^{j\Psi_k}, \quad (3.47)$$

where

$$\Psi_k = \mathbf{P}_k \mathbf{W}_1 \Theta_1 \mathbf{W}_1^T \mathbf{P}_k^T. \quad (3.48)$$

# Chapter 4

## CMR Filter Synthesis Using Field

### Coupling Formalism

The filter synthesis problem is to determine the coupling topology and coupling coefficients of the microring structure that can realize a prescribed optical transfer function, and can be regarded as the inverse of the analysis problem. As a result, the synthesis problem is typically more difficult than the analysis problem, and does not always have solutions. Different methods for synthesizing various microring filters have been developed based on various approaches. A popular approach of microring filter synthesis utilizes techniques from the mature field of microwave filter design and applies them to an appropriate narrowband model of coupled microring resonators [10]. Other design techniques based on pole-zero dynamics [40] or parameter optimizations [41] have also been proposed; however, these methods require numerical optimizations. A direct synthesis method which does not require optimization is more desirable since it can exactly realize a prescribed filter transfer function and often provides more realistic parameters.

Microring filter synthesis can be carried out in either the complex frequency

domain ( $s$ -domain) or the unit delay variable domain ( $z$ -domain). While the energy coupling formalism generally provides simpler equations than the field coupling formalism, its synthesis method is less accurate for broadband CMR devices due to its assumption of weak coupling. Therefore there is a need to develop a more rigorous synthesis procedure based on field coupling for applications in designing broadband devices.

#### 4.1 General 2D-CMR field coupling synthesis

In this section, we develop a procedure for synthesizing 2D-CMR networks based on the inverse problem of the field coupling analysis. The synthesis procedure developed should be applicable to general 2D-CMR networks for realizing high order filter responses. Part of the work has been presented in [39].

##### 4.1.1 Description of the CMR network

Similar to Figure 3.1, the general schematic of a 2D CMR network consists of  $N$  coupled and identical microring resonators as shown in Figure 4.1(a). The

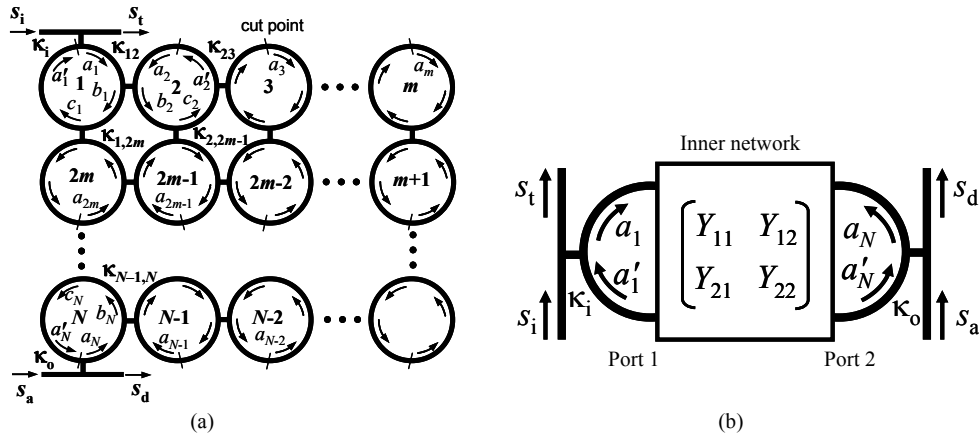


Figure 4.1 – (a) Schematic of a general 2D coupled microring array with  $N$  microrings; (b) inner CMR network.

same field labelling scheme is also applied, where we follow the direction of wave propagation in each microring  $i$  and label the field amplitudes as  $a_i, b_i, c_i, d_i$  as shown in the figure. The field coupling coefficient between adjacent microrings  $i$  and  $j$  is denoted by  $\kappa_{ij}$ . Microrings 1 and  $N$  are also coupled to the input and output bus waveguides, respectively, via coupling coefficients  $\kappa_i$  and  $\kappa_o$ . The input and output signals of the network are labelled  $s_i$  (input),  $s_t$  (through),  $s_d$  (drop) and  $s_a$  (add). We define the transfer matrix  $\mathbf{S}$  relating the output and input signals as

$$\begin{bmatrix} s_t \\ s_d \end{bmatrix} = \begin{bmatrix} S_{11} & S_{12} \\ S_{21} & S_{22} \end{bmatrix} \begin{bmatrix} s_i \\ s_a \end{bmatrix}. \quad (4.1)$$

From equations (3.14), (3.17), (3.19a) and (3.19b), the transfer functions at the through port ( $S_{11}$ ) and drop port ( $S_{21}$ ) of the device can be expressed as ratios of polynomials of the roundtrip delay variable  $z^{-1} = e^{-j\phi_{\text{rt}}}$ , where  $\phi_{\text{rt}}$  is the roundtrip phase of the microring, as

$$S_{11}(z^{-1}) = \frac{s_t}{s_i} = \frac{\sum_{k=0}^N r_k z^{-k}}{1 + \sum_{k=1}^N q_k z^{-k}} \equiv \frac{R(z^{-1})}{Q(z^{-1})}, \quad (4.2a)$$

$$S_{21}(z^{-1}) = \frac{s_d}{s_i} = \frac{j \sum_{k=0}^{N-2} p_k z^{-k}}{1 + \sum_{k=1}^N q_k z^{-k}} \equiv \frac{jP(z^{-1})}{Q(z^{-1})}. \quad (4.2b)$$

Since the microring network can be regarded as a lossless digital network, we also have  $S_{22} = \tilde{R}/Q$  and  $S_{12} = j\tilde{P}/Q$ , where  $\tilde{R}$  and  $\tilde{P}$  are the

para-conjugate polynomials of  $R$  and  $P$  obtained by reversing the coefficients of the respective polynomials [42,43]. In the synthesis problem, given the polynomials  $P$ ,  $R$ , and  $Q$  of the prescribed transfer function, we would like to determine the coupling topology and the coupling coefficients of the CMR network that could achieve the desired filter spectral response.

To facilitate the synthesis, we define an inner CMR network without the input and output coupling buses, as shown in Figure 4.1(b). The input and output signals of the inner network are given by  $[a_1, a'_1]$  at port 1 and  $[a_N, a'_N]$  at port 2, where  $a'_1$  and  $a'_N$  are the signals just before the input and output coupling junctions, respectively. We define a Y-parameter matrix which characterizes the behaviour of the inner CMR network by relating its input and output signals as

$$\begin{bmatrix} a'_1 \\ a'_N \end{bmatrix} = \begin{bmatrix} Y_{11} & Y_{12} \\ Y_{21} & Y_{22} \end{bmatrix} \begin{bmatrix} a_1 \\ a_N \end{bmatrix}. \quad (4.3)$$

The Y-parameters of the inner network can be related to the S-parameters of the total CMR network as follows. At the input coupling junction, we have the following relations between the bus signals  $s_i$  and  $s_t$  and the fields in ring 1 ( $a_1$  and  $a'_1$ ):

$$a_1 = \tau_i a'_1 - j\kappa_i s_i, \quad (4.4a)$$

$$s_t = \tau_i s_i - j\kappa_i a'_1, \quad (4.4b)$$

where  $\tau_i = \sqrt{1 - \kappa_i^2}$ . Solving (4.4b) for  $a'_1$ , and substituting into (4.4a) we have

$$a'_1 = (\tau_i s_i - s_i)/(j\kappa_i), \quad (4.4c)$$

$$a_1 = (s_i - \tau_i s_i)/(j\kappa_i). \quad (4.4d)$$

Similar expressions can also be found for the output coupling junction:

$$a_N = \tau_o a'_N - j\kappa_o s_a, \quad (4.5a)$$

$$s_d = \tau_o s_a - j\kappa_o a'_N, \quad (4.5b)$$

or

$$a'_N = (\tau_o s_a - s_d)/(j\kappa_o), \quad (4.5c)$$

$$a_N = (s_a - \tau_o s_d)/(j\kappa_o), \quad (4.5d)$$

where  $\tau_o = \sqrt{1 - \kappa_o^2}$ . Using (4.3) – (4.5), we can relate the S-parameters of the total network to the inner network Y-parameters. First, from equation (4.3) we have:

$$a'_1 = Y_{11} a_1 + Y_{12} a_N, \quad (4.6a)$$

$$a'_N = Y_{21} a_1 + Y_{22} a_N. \quad (4.6b)$$

Using equations (4.4c,d) and (4.5c,d) we eliminate  $a'_1, a'_N, a_1, a_N$  from (4.6a) and (4.6b) to get

$$\frac{\tau_i Y_{11} - 1}{j\kappa_i} s_i + \frac{\tau_o Y_{12}}{j\kappa_o} s_d = \frac{Y_{11} - \tau_i}{j\kappa_i} s_i + \frac{Y_{12}}{j\kappa_o} s_a, \quad (4.7a)$$

$$\frac{\tau_i Y_{21}}{j\kappa_i} s_i + \frac{\tau_o Y_{22} - 1}{j\kappa_o} s_d = \frac{Y_{21}}{j\kappa_i} s_i + \frac{Y_{22} - \tau_o}{j\kappa_o} s_a. \quad (4.7b)$$

Using (4.7a) and (4.7b) and setting  $s_a = 0$  we solve for  $s_i$  and  $s_d$  in terms of  $s_i$  to get:

$$S_{11} = \left. \frac{s_t}{s_i} \right|_{s_a=0} = \frac{(Y_{11} - \tau_o \Delta_Y) - \tau_i (1 - \tau_o Y_{22})}{\tau_i (Y_{11} - \tau_o \Delta_Y) - (1 - \tau_o Y_{22})}, \quad (4.8a)$$

$$S_{21} = \left. \frac{s_d}{s_i} \right|_{s_a=0} = \frac{\kappa_i \kappa_o Y_{21}}{\tau_i (Y_{11} - \tau_o \Delta_Y) - (1 - \tau_o Y_{22})}, \quad (4.8b)$$

where  $\Delta_Y = Y_{11}Y_{22} - Y_{12}Y_{21}$  is the determinant of the Y-parameter matrix.

We now consider the network under the condition  $\tau_o = 1$ . This is equivalent to removing the output bus waveguide so that the CMR network becomes an all-pass network with input  $s_i$  and output  $s_t$ . The all-pass transfer function can be obtained by setting  $\tau_o = 1$  in (4.8a),

$$S_{11}^{\text{ap}} = \left. \frac{s_t}{s_i} \right|_{\tau_o=1} = \frac{(Y_{11} - \Delta_Y) - \tau_i (1 - Y_{22})}{\tau_i (Y_{11} - \Delta_Y) - (1 - Y_{22})}. \quad (4.9)$$

From the digital two-port network perspective, the all-pass transfer function is simply the reflection coefficient of the network, which is given in terms of the  $S_{11}$  parameter as

$$S_{11}^{\text{ap}} = \frac{1 + \tilde{S}_{11}}{1 + S_{11}} = \frac{\tilde{Q} + \tilde{R}}{Q + R}. \quad (4.10)$$

For the inner CMR network, the condition  $\tau_o = 1$  implies that  $a'_N = a_N$  (i.e. no change as the signal passes through the junction). Setting  $a'_N = a_N$  in (4.3) we can obtain the following expressions:

$$Y_{11}^{\text{ap}} = \left. \frac{a'_1}{a_1} \right|_{a'_N=a_N} = \frac{1 - Y_{22}}{Y_{11} - \Delta_Y}, \quad (4.11a)$$

$$Y_{21}^{\text{ap}} = \left. \frac{a'_N}{a_1} \right|_{a'_N=a_N} = \frac{Y_{21}}{Y_{11} - \Delta_Y}. \quad (4.11\text{b})$$

By dividing the numerator and denominator of (4.9) by  $Y_{11} - \Delta_Y$  and using (4.11a), we obtain

$$S_{11}^{\text{ap}} = \frac{1 - \tau_i Y_{11}^{\text{ap}}}{\tau_i - Y_{11}^{\text{ap}}}, \quad (4.12)$$

or

$$Y_{11}^{\text{ap}} = \frac{1 - \tau_i S_{11}^{\text{ap}}}{\tau_i - S_{11}^{\text{ap}}}. \quad (4.13)$$

Upon substitution of (4.10) into the above, we get

$$Y_{11}^{\text{ap}} = \frac{(Q + R) - \tau_i (\tilde{Q} + \tilde{R})}{\tau_i (Q + R) - (\tilde{Q} + \tilde{R})}. \quad (4.14)$$

As for the expression for  $Y_{21}^{\text{ap}}$  in (4.11b), we recognize that it has the same denominator as  $Y_{11}^{\text{ap}}$  and the same numerator as  $Y_{21}$ . From (4.8b) we also see that  $Y_{21}$ , and hence  $Y_{21}^{\text{ap}}$ , has the same zeros as  $S_{21}$ . Thus we can express  $Y_{21}^{\text{ap}}$  as

$$Y_{21}^{\text{ap}} = \frac{kP}{\tau_i (Q + R) - (\tilde{Q} + \tilde{R})}, \quad (4.15)$$

where  $k$  is some constant. Equations (4.14) and (4.15) allow us to construct the all-pass Y-parameters of the inner CMR network from the polynomials  $P$ ,  $R$  and  $Q$  of the given optical transfer functions.

### 4.1.2 Field coupling synthesis of CMR networks

It has already been shown in Section 3.1 that the CMR network in Figure 4.1(a) can be characterized by a field coupling matrix  $\mathbf{M}$  which is constructed from the ring-to-ring field coupling elements  $\kappa_{i,j}$ . The goal of this section is to derive expressions linking the coupling matrix  $\mathbf{M}$  with the all-pass Y-parameters  $Y_{11}^{\text{ap}}$  and  $Y_{21}^{\text{ap}}$  of the inner network. A procedure for constructing  $\mathbf{M}$  will then be described.

Similar to the procedure presented in Section 3.1, we first transform the CMR structure into an equivalent coupled waveguide array and obtain the ring-to-ring field coupling matrix,  $\mathbf{M}$ , of the CMR network as presented in equation (3.7).

For microring 1, at the input bus coupling junction, we can combine (4.4a) and (4.4b) to get  $a_1 = a'_1 + u_1$ , where

$$u_1 = \frac{1 - \tau_i}{j\kappa_i} (s_i + s_t). \quad (4.16)$$

Similarly for microring  $N$ , at the output bus coupling junction we have  $a_N = a'_N + u_N$ , with

$$u_N = \frac{1 - \tau_o}{j\kappa_o} (s_a + s_d). \quad (4.17)$$

Thus in general we can write  $\mathbf{a} = \mathbf{a}' + \mathbf{u}$ , where  $\mathbf{u} = [u_1, 0, \dots, 0, u_N]^T$ .

Substituting this expression into (3.7) we get  $\mathbf{a} - \mathbf{u} = z^{-1}\mathbf{M}\mathbf{a}$ , or

$$(\mathbf{I} - z^{-1}\mathbf{M})\mathbf{a} = \mathbf{u}, \quad (4.18)$$

where  $\mathbf{I}$  is the  $N \times N$  identity matrix. In the above equation the term on the left hand side completely characterizes the inner CMR network, whereas the right hand side accounts for the external effects of the input and output bus couplings  $\kappa_i$  and  $\kappa_o$ .

Assuming lossless coupling between adjacent microrings, the conservation of power requires that the coupling matrices  $\mathbf{M}_k$  be unitary. It follows that the total field coupling matrix  $\mathbf{M}$  is also unitary and normal so that its eigenvectors are orthogonal to each other. Thus we can diagonalize  $\mathbf{M}$  as  $\mathbf{M} = \mathbf{T}\mathbf{\Lambda}\mathbf{T}^H$ , where  $\mathbf{\Lambda}$  is a diagonal matrix containing the eigenvalues of  $\mathbf{M}$  and  $\mathbf{T}$  is a unitary matrix containing the corresponding eigenvectors. Substituting this into (4.18) gives

$$(\mathbf{I} - z^{-1}\mathbf{T}\mathbf{\Lambda}\mathbf{T}^H)\mathbf{a} = \mathbf{u}, \quad (4.19)$$

and we can solve for  $\mathbf{a}$  to get

$$\mathbf{a} = \mathbf{T}(\mathbf{I} - z^{-1}\mathbf{\Lambda})^{-1}\mathbf{T}^H\mathbf{u} \equiv \mathbf{A}\mathbf{u}, \quad (4.20)$$

where  $\mathbf{A}$  is an  $N \times N$  matrix defined as in the above equation. From (4.20) we obtain the following expressions for  $a_1$  and  $a_N$ :

$$\begin{aligned} a_1 &= A_{11}u_1 + A_{1N}u_N \\ &= u_1 \sum_{k=1}^N \frac{|T_{1,k}|^2}{1 - \lambda_k z^{-1}} + u_N \sum_{k=1}^N \frac{T_{1,k} T_{N,k}^*}{1 - \lambda_k z^{-1}}, \end{aligned} \quad (4.21a)$$

$$\begin{aligned} a_N &= A_{N1}u_1 + A_{NN}u_N \\ &= u_1 \sum_{k=1}^N \frac{T_{N,k} T_{1,k}^*}{1 - \lambda_k z^{-1}} + u_N \sum_{k=1}^N \frac{|T_{N,k}|^2}{1 - \lambda_k z^{-1}}, \end{aligned} \quad (4.21b)$$

where  $\lambda_k$ 's are the eigenvalues of  $\mathbf{M}$ . For the all-pass CMR network with no

output bus waveguide, setting  $\tau_0 = 1$  in (4.17) gives  $u_N = 0$ . Under this condition we obtain from (4.21a) and (4.21b)

$$A_{11} = \frac{a_1}{u_1} \Big|_{u_N=0} = \sum_{k=1}^N \frac{|T_{1,k}|^2}{1 - \lambda_k z^{-1}}, \quad (4.22a)$$

$$A_{N1} = \frac{a_N}{u_1} \Big|_{u_N=0} = \sum_{k=1}^N \frac{T_{N,k} T_{1,k}^*}{1 - \lambda_k z^{-1}}. \quad (4.22b)$$

Moreover, since  $u_1 = a_1 - a'_1$ , we also have

$$A_{11} = \frac{a_1}{u_1} = \frac{a_1}{a_1 - a'_1} = \frac{1}{1 - Y_{11}^{\text{ap}}}, \quad (4.23a)$$

and similarly,

$$A_{N1} = \frac{a_N}{u_1} = \frac{a_N}{a_1 - a'_1} = \frac{Y_{21}^{\text{ap}}}{1 - Y_{11}^{\text{ap}}}. \quad (4.23b)$$

Finally, substituting (4.14) and (4.15) into the above expressions, we obtain

$$A_{11} = \frac{1}{1 - \tau_i} \frac{(\tilde{Q} + \tilde{R}) - \tau_i(Q + R)}{(\tilde{Q} + \tilde{R}) + (Q + R)} \equiv \frac{N_{11}(z^{-1})}{D(z^{-1})}, \quad (4.24a)$$

$$A_{N1} = \frac{k}{1 - \tau_i} \frac{P}{(\tilde{Q} + \tilde{R}) + (Q + R)} \equiv \frac{N_{21}(z^{-1})}{D(z^{-1})}. \quad (4.24b)$$

Equations (4.22a) and (4.22b) provide a link between the polynomials of the transfer functions of the CMR network and the eigenvalues and eigenvectors of the coupling matrix  $\mathbf{M}$ . In the next subsection, we discuss how the matrix  $\mathbf{M}$  can be constructed from the prescribed optical transfer functions.

### 4.1.3 Constructing the coupling matrix $\mathbf{M}$

Given the polynomials  $P$ ,  $R$  and  $Q$ , as in (4.2a) and (4.2b), of the prescribed optical transfer functions ( $S_{21}$  and  $S_{11}$ ) at the drop port and through port of the CMR network, we can determine the bus coupling coefficients  $\kappa_i$  and  $\kappa_o$  and construct the coupling matrix  $\mathbf{M}$  of the network as follows. Since  $\mathbf{T}$  is a unitary matrix, its columns have unity magnitude. For the first column, we have

$$\sum_{k=1}^N |T_{1,k}|^2 = 1. \quad (4.25)$$

From (4.22a), we recognize that the above expression is also the zeroth order coefficient of the numerator polynomial of  $A_{11}$ . Enforcing this condition to the right hand side expression in (4.24a), we obtain

$$\tau_i = \frac{q_N + r_N}{1 + r_0}. \quad (4.26)$$

For filters with symmetric spectral responses, the CMR network is also symmetric so that  $\tau_o = \tau_i$  (or  $\kappa_o = \kappa_i$ ). Knowledge of  $\tau_i$  allows us to compute the polynomials  $N_{11}$ ,  $N_{21}$  and  $D$  as defined in (4.24a) and (4.24b). Performing partial fraction expansions of the rational functions  $N_{11}/D$  and  $N_{21}/D$ , we can write

$$\frac{N_{11}(z^{-1})}{D(z^{-1})} = \sum_{k=1}^N \frac{\xi_k^{(11)}}{\rho_k - z^{-1}}, \quad (4.27a)$$

$$\frac{N_{21}(z^{-1})}{D(z^{-1})} = \sum_{k=1}^N \frac{\xi_k^{(21)}}{\rho_k - z^{-1}}, \quad (4.27b)$$

where  $\rho_k$  are the poles and  $\xi_k^{(11)}$  and  $\xi_k^{(21)}$  are the residues of the respective rational function. Comparing (4.27a) and (4.27b) with (4.22a) and (4.22b) shows that the inverse of the poles,  $1/\rho_k$ , are the eigenvalues  $\lambda_k$  of the matrix  $\mathbf{M}$ .

The elements  $T_{1,k}$  and  $T_{N,k}$  of the first and last rows, respectively, of  $\mathbf{T}$  are obtained from the residues  $\xi_k^{(11)}$  and  $\xi_k^{(21)}$  as

$$T_{1,k} = \left| \xi_k^{(11)} / \rho_k \right|^{1/2}, \quad (4.28a)$$

$$T_{N,k} = \frac{\xi_k^{(21)}}{\rho_k T_{1,k}}. \quad (4.28b)$$

The remaining rows of  $\mathbf{T}$  are obtained by Gram-Schmidt orthogonalization [5]. The total field coupling matrix  $\mathbf{M}$  is then obtained from  $\mathbf{M} = \mathbf{T}\mathbf{\Lambda}\mathbf{T}^H$ .

#### 4.1.4 Determining the CMR network topology and coupling coefficients

From the coupling matrix  $\mathbf{M}$  we can then proceed to determine the device topology and the corresponding coupling coefficients of the CMR network. This is achieved by first determining the coupling-angle matrix  $\mathbf{\Psi}$  such that  $\mathbf{M} = \exp(j\mathbf{\Psi})$ . Since  $\mathbf{M}$  is normal, its eigenvalues have unity magnitude so  $\mathbf{\Lambda}$  can be expressed as  $\mathbf{\Lambda} = \exp(j\mathbf{\Theta})$ . The coupling-angle matrix is then obtained from  $\mathbf{\Psi} = \mathbf{T}\mathbf{\Theta}\mathbf{T}^H$ . The element  $\Psi_{ij}$  gives the coupling angle between microrings  $i$  and  $j$ , with the coupling coefficient equal to  $\kappa_{ij} = \sin(\Psi_{ij})$ . The matrix  $\mathbf{\Psi}$  initially obtained from the above procedure is in general a full matrix, which is not physically realizable since it requires each microring in the network to be coupled to every other microring. In order to reduce  $\mathbf{\Psi}$  to a simpler and realizable microring coupling topology, we employ a procedure similar to the energy-coupling synthesis of 2D-CMRs [5] where a series of Jacobi matrix

rotations is applied to  $\Psi$  to eliminate as many coupling elements as possible. It has already been shown in Section 3.3 that such similarity transformation is also applicable to the field coupling formulation of CMRs without disturbing the device response. By applying successive rotations to the matrix  $\Psi$  to eliminate as many coupling angles as possible, a final matrix can then be obtained which gives the optimized coupling topology and the corresponding coupling angles of the CMR.

#### 4.1.5 Design example: a 6<sup>th</sup>-order optical filter

As an example to illustrate the synthesis procedure developed above, we consider the design of a broadband optical filter with a 3dB bandwidth of 250GHz

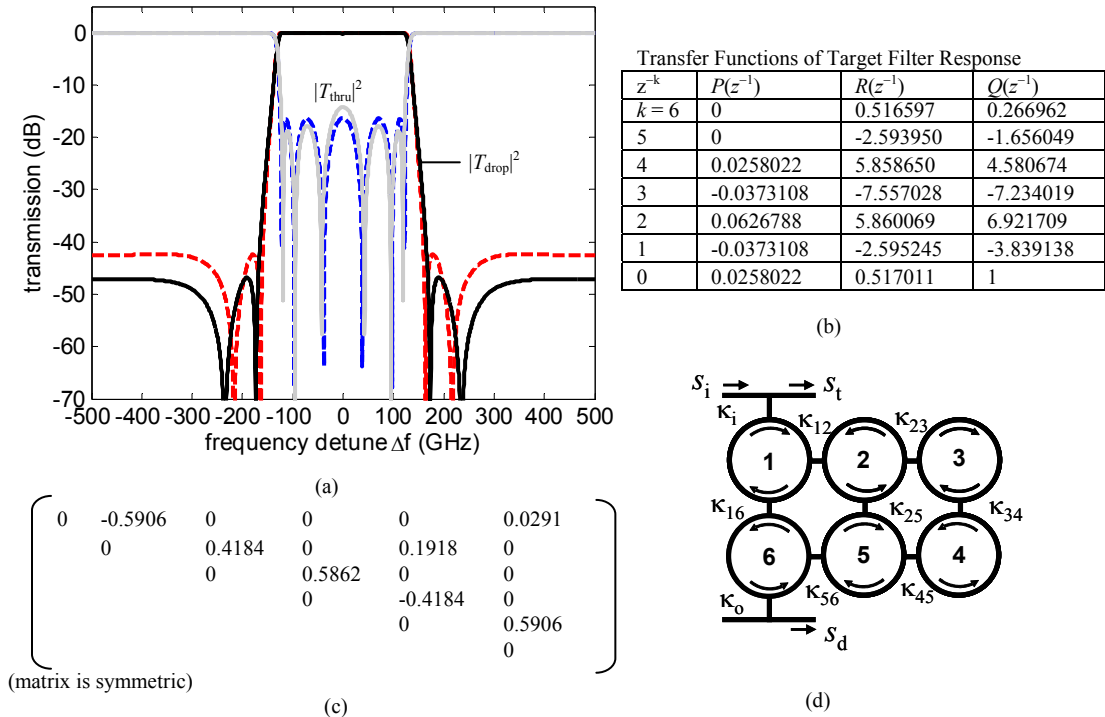


Figure 4.2. (a) Target filter responses (dashed lines) and responses of the synthesized CMR network (solid lines). (b) Polynomials of the transfer functions of the target filter. (c) Coupling-angle matrix and (d) coupling topology of the synthesized CMR network. [39]

using microring resonators with 1THz FSR. The in-band ripples are 0.1dB and the stop-band rejection is specified to be better than 40dB. Using an appropriate filter approximation method [44], the transfer functions of a sixth-order filter satisfying the above specifications are obtained as given by the polynomials in Figure 4.2(b). The desired target through-port and drop-port spectral responses are shown by the dashed lines in Figure 4.2(a). Using equation (4.26), the computed bus-to-ring coupling coefficients of the CMR network are  $\kappa_i = \kappa_o = 0.8563$ . The coupling-angle matrix  $\Psi$  after optimization and the corresponding CMR coupling topology are shown in Figures 4.2(c) and (d). The spectral responses of the synthesized CMR network are also plotted in Figure 4.2(a) (solid lines), which shows good agreement with the target filter responses. The small discrepancies are due to the fact that in constructing the coupling-angle matrix  $\Psi$  from the matrix  $\mathbf{M}$ , we have neglected the fact that  $\mathbf{M}$  is actually a cascade of 4 coupling matrices  $\mathbf{M}_k$  in the coupled-waveguide array. This is equivalent to neglecting the effect of indirect couplings between the microrings, which arise from the non-commutative nature of the matrices  $\mathbf{M}_k$  [30, 31, 39].

## 4.2 Synthesis of 2xN CMRs by network order reduction

While the synthesis method presented in Section 4.1 can be used to synthesize general 2D-CMR networks, a difficulty which arises in the method is the determination of the coupling topology and the coupling coefficients from the field coupling matrix  $\mathbf{M}$ . A solution to this problem has not been found unless the indirect coupling matrix  $\mathbf{X}$  is neglected, as was done in the example. Due to this approximation, the synthesized filter response does not exactly match with

the prescribed response, as seen in Figure 4.2(a).

We have also developed an alternative synthesis approach which can exactly realize the prescribed filter response. The method is based on the network order reduction approach, and is at the present limited to the  $2 \times N$  microring coupling topology. However, this is not a serious limitation, since any general 2D microring coupling topology of order  $2N$  can be reduced to the  $2 \times N$  configuration via appropriate similarity transformations [5]. The network order reduction technique has previously been used to synthesize microring filters of simple one dimensional coupling topology (e.g., CROWs) [9], cascaded arrays of ring-loaded Mach-Zehnder interferometers [7], and parallel cascades of microring networks [45]. Here we show that the method can also be applied to synthesize 2D-CMR networks of the  $2 \times N$  coupling topology. This work has been published in [46].

#### 4.2.1 Description of the $2 \times N$ CMR network

A general schematic of a  $2 \times N$  CMR network consisting of  $2N$  coupled microring resonators is shown in Figure 4.3. The microring resonators are numbered from 1 to  $2N$  as shown, and are assumed to be identical and lossless. The field coupling coefficient between adjacent microrings  $i$  and  $j$  is denoted by  $\kappa_{i,j}$ . Input and output bus waveguides are coupled to the network via microrings  $N$  and  $2N$ , with coupling coefficients  $\kappa_i$  and  $\kappa_o$  respectively. We denote the input and output signals of the network as  $s_i$  (input),  $s_t$  (through),  $s_d$  (drop) and  $s_a$  (add) as shown in the figure. The transfer matrix  $\mathbf{S}$  of the network is defined as

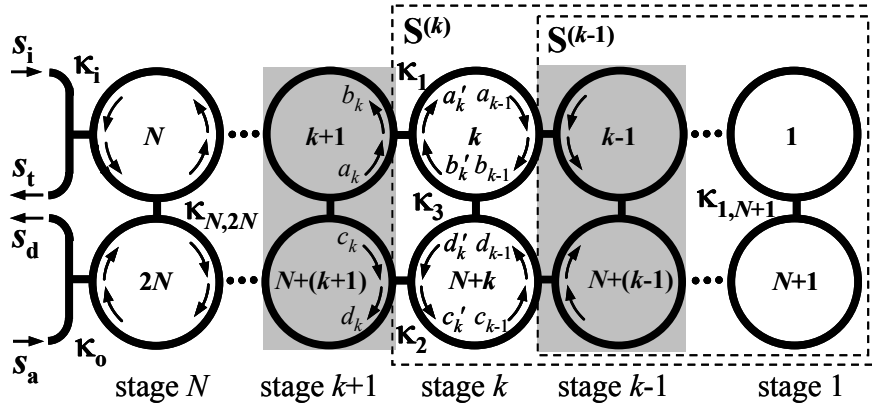


Figure 4.3 . Schematic of a  $2 \times N$  CMR network and its depiction as a cascade of  $N$  stages of microring pairs. [46]

$$\begin{bmatrix} s_t \\ s_d \end{bmatrix} = \begin{bmatrix} S_{11} & S_{12} \\ S_{21} & S_{22} \end{bmatrix} \begin{bmatrix} s_i \\ s_a \end{bmatrix}, \quad (4.29)$$

in which the transfer functions at the through port ( $S_{11}$ ) and drop port ( $S_{21}$ ) can be expressed as ratios of polynomials of the roundtrip delay variable  $z^{-1}$  similar to equations (4.2a) and (4.2b):

$$S_{11}(z^{-1}) = \frac{s_t}{s_i} = \frac{\sum_{k=0}^{2N} r_k z^{-k}}{1 + \sum_{k=1}^{2N} q_k z^{-k}} \equiv \frac{R(z^{-1})}{Q(z^{-1})}, \quad (4.30a)$$

$$S_{21}(z^{-1}) = \frac{s_d}{s_i} = \frac{jz^{-1} \sum_{k=0}^{2N-2} p_{k+1} z^{-k}}{1 + \sum_{k=1}^{2N} q_k z^{-k}} \equiv \frac{jP(z^{-1})}{Q(z^{-1})}. \quad (4.30b)$$

For the network of order  $2N$ , transmission response at the drop port has  $2N$  poles and  $2N - 2$  zeros, while the through-port response has  $2N$  poles and  $2N$  zeros. For most optical filters of practical interest, the spectral responses are symmetric about the center frequency, in which case we also have the relations

$S_{22} = S_{11} = R/Q$  and  $S_{12} = S_{21} = jP/Q$ . In addition, power conservation requires that the determinant of the transfer matrix  $\mathbf{S}$  obeys the relation [7, 43]

$$S_{11}S_{22} - S_{12}S_{21} = \frac{R^2 + P^2}{Q^2} = \frac{Q\tilde{Q}}{Q^2} = \frac{\tilde{Q}}{Q}, \quad (4.31)$$

where  $\tilde{Q}$  is the para-conjugate polynomial of  $Q$  obtained by reversing its coefficients.

#### 4.2.2 Network order reduction

The idea of the network order reduction method is based on regarding the  $2 \times N$  CMR network as a cascade of  $N$  stages and synthesizing each stage one by one by extracting it from the cascaded array. The order of the network is reduced each time a stage is synthesized and removed from the cascade, until the last stage is reached. For the  $2 \times N$  CMR network, each stage consists of a pair of coupled microrings as shown in Figure 4.3, and we number the stages as  $k = 1, 2, \dots, N$  starting from the right most pair. The transfer matrix  $\mathbf{S}^{(k)}$  of the  $2 \times k$  CMR network formed by microring pairs 1 to  $k$  is defined as

$$\begin{bmatrix} b_k \\ d_k \end{bmatrix} = \begin{bmatrix} S_{11}^{(k)} & S_{12}^{(k)} \\ S_{21}^{(k)} & S_{22}^{(k)} \end{bmatrix} \begin{bmatrix} a_k \\ c_k \end{bmatrix} = \frac{1}{Q_k} \begin{bmatrix} R_k & jP_k \\ jP_k & R_k \end{bmatrix} \begin{bmatrix} a_k \\ c_k \end{bmatrix} \quad (4.32)$$

where  $Q_k$  and  $R_k$  are polynomials of degree  $2k$  and  $P_k$  is of degree  $2k - 1$ . We next derive the relationships between the  $S$ -parameters of the  $2 \times k$  network and the previous network,  $2 \times (k-1)$  in the following.

As seen in Figure 4.3, networks  $2 \times k$  and  $2 \times (k-1)$  are connected by the microring pair in stage  $k$ . For convenience, we re-label the three coupling

coefficients of this stage as  $\kappa_1$ ,  $\kappa_2$  and  $\kappa_3$ , and define the fields inside the microrings as shown in the same figure. At the coupling junctions  $\kappa_1$  and  $\kappa_2$  we have the relations

$$\begin{bmatrix} b_k \\ a'_k \end{bmatrix} = \begin{bmatrix} \tau_1 & -j\kappa_1 \\ -j\kappa_1 & \tau_1 \end{bmatrix} \begin{bmatrix} a_k \\ b'_k \end{bmatrix}, \quad (4.33a)$$

$$\begin{bmatrix} d_k \\ c'_k \end{bmatrix} = \begin{bmatrix} \tau_2 & -j\kappa_2 \\ -j\kappa_2 & \tau_2 \end{bmatrix} \begin{bmatrix} c_k \\ d'_k \end{bmatrix}, \quad (4.33b)$$

and at the coupling junction  $\kappa_3$ ,

$$\begin{bmatrix} b'_k \\ d'_k \end{bmatrix} = z^{-1/2} \begin{bmatrix} \tau_3 & -j\kappa_3 \\ -j\kappa_3 & \tau_3 \end{bmatrix} \begin{bmatrix} b_{k-1} \\ d_{k-1} \end{bmatrix}, \quad (4.33c)$$

where  $\tau_i = \sqrt{1 - \kappa_i^2}$  (for  $i = 1, 2, 3$ ). Using the relations  $a_{k-1} = z^{-1/2} a'_k$  and  $c_{k-1} = z^{-1/2} c'_k$ , we eliminate the fields  $a'_k, b'_k, c'_k, d'_k$  from (4.33a)-(4.33c) and express the results in the form

$$\begin{bmatrix} b_{k-1} \\ d_{k-1} \end{bmatrix} = \begin{bmatrix} S_{11}^{(k-1)} & S_{12}^{(k-1)} \\ S_{21}^{(k-1)} & S_{22}^{(k-1)} \end{bmatrix} \begin{bmatrix} a_{k-1} \\ c_{k-1} \end{bmatrix}. \quad (4.34)$$

Specifically, the parameters  $S_{11}^{(k-1)}$  and  $S_{21}^{(k-1)}$  are given by

$$S_{11}^{(k-1)} = z \frac{\tau_3(\tau_2 \Delta_k - S_{11}^{(k)} - \tau_1 \tau_2 S_{22}^{(k)} + \tau_1) - j\kappa_1 \kappa_2 \kappa_3 S_{21}^{(k)}}{\tau_1 \tau_2 \Delta_k - \tau_1 S_{11}^{(k)} - \tau_2 S_{22}^{(k)} + 1}, \quad (4.35a)$$

$$S_{21}^{(k-1)} = z \frac{j\kappa_3(\tau_2 \Delta_k - S_{11}^{(k)} - \tau_1 \tau_2 S_{22}^{(k)} + \tau_1) - \kappa_1 \kappa_2 \tau_3 S_{21}^{(k)}}{\tau_1 \tau_2 \Delta_k - \tau_1 S_{11}^{(k)} - \tau_2 S_{22}^{(k)} + 1}, \quad (4.35b)$$

where  $\Delta_k$  is the determinant of  $\mathbf{S}^{(k)}$ ,

$$\Delta_k = S_{11}^{(k)} S_{22}^{(k)} - S_{12}^{(k)} S_{21}^{(k)} = \tilde{Q}_k / Q_k. \quad (4.36)$$

Using (4.32) in (4.35a) and (4.35b) we can obtain the following recursive relations connecting the transfer polynomials of network  $2 \times k$  with those of the previous network:

$$Q_{k-1} = \tau_1 \tau_2 \tilde{Q}_k - (\tau_1 + \tau_2) R_k + Q_k, \quad (4.37a)$$

$$R_{k-1} = z(\tau_3 M_k + \kappa_1 \kappa_2 \kappa_3 P_k), \quad (4.37b)$$

$$P_{k-1} = z(\kappa_3 M_k - \kappa_1 \kappa_2 \tau_3 P_k), \quad (4.37c)$$

where

$$M_k = \tau_2 \tilde{Q}_k - (1 + \tau_1 \tau_2) R_k + \tau_1 Q_k. \quad (4.37d)$$

The transmission coefficients  $\tau_1$ ,  $\tau_2$  and  $\tau_3$  of stage  $k$  can be determined by considering the degrees of the polynomials in the above equations. Since  $Q_{k-1}$  has degree  $2(k-1)$ , we require the coefficients of the  $z^{-2k}$  and  $z^{-(2k-1)}$  terms in (4.37a) to be zero:

$$\tau_1 \tau_2 - (\tau_1 + \tau_2) r_{2k}^{(k)} + q_{2k}^{(k)} = 0, \quad (4.38a)$$

$$\tau_1 \tau_2 q_1^{(k)} - (\tau_1 + \tau_2) r_{2k-1}^{(k)} + q_{2k-1}^{(k)} = 0, \quad (4.38b)$$

where  $q_i^{(k)}$  and  $r_i^{(k)}$  are the  $i^{\text{th}}$  coefficients of  $Q_k$  and  $R_k$ , respectively. Solving for  $\tau_1$  and  $\tau_2$  from the above equations we get

$$\tau_1, \tau_2 = \frac{B \pm \sqrt{B^2 - 4A}}{2}, \quad (4.39)$$

where

$$A = \frac{r_{2k}^{(k)} q_{2k-1}^{(k)} - r_{2k-1}^{(k)} q_{2k}^{(k)}}{r_{2k-1}^{(k)} - r_{2k}^{(k)} q_1^{(k)}}, \quad (4.40a)$$

$$B = \frac{q_{2k-1}^{(k)} - q_1^{(k)} q_{2k}^{(k)}}{r_{2k-1}^{(k)} - r_{2k}^{(k)} q_1^{(k)}}. \quad (4.40b)$$

For filters with symmetric spectral responses, it turns out that  $B^2 - 4A = 0$  so that  $\tau_1 = \tau_2 = B/2$ . For the polynomial  $R_{k-1}$  in (4.37b), which also has degree  $2(k-1)$ , we require the  $z^{+1}$  and  $z^{-(2k-1)}$  terms to be zero. This implies that the  $z^0$  and  $z^{-2k}$  terms of  $M_k$  in (4.37d) must be zero,

$$m_0^{(k)} = \tau_2 q_{2k}^{(k)} - (1 + \tau_1 \tau_2) r_0^{(k)} + \tau_1 = 0, \quad (4.41a)$$

$$m_{2k}^{(k)} = \tau_2 - (1 + \tau_1 \tau_2) r_{2k}^{(k)} + q_{2k}^{(k)} \tau_1 = 0. \quad (4.41b)$$

The above equations provide an alternative expression for determining  $\tau_1$  and  $\tau_2$ ,

$$\tau_1 = \tau_2 = C - \sqrt{C^2 - 1}, \quad (4.42)$$

where  $C = [1 + q_{2k}^{(k)}] / 2r_0^{(k)}$ . Finally, since  $P_{k-1}$  has degree  $2k - 3$ , by requiring that the coefficient of the  $z^{-(2k-2)}$  term in (4.37c) to be zero, we obtain

$$\kappa_3 m_{2k-1}^{(k)} - \kappa_1 \kappa_2 \tau_3 p_{2k-1}^{(k)} = 0, \quad (4.43)$$

which can be solved for  $\kappa_3$  to get

$$\kappa_3 = \sin \left[ \tan^{-1} \left( \frac{\kappa_1 \kappa_2 p_{2k-1}^{(k)}}{m_{2k-1}^{(k)}} \right) \right]. \quad (4.44)$$

In the synthesis procedure, we start with the prescribed optical transfer functions  $S_{11}^{(N)}$  and  $S_{21}^{(N)}$  to be realized by a  $2 \times N$  CMR network. First, we compute the coupling coefficients of the last stage ( $k = N$ ) to obtain the input and output bus coupling coefficients ( $\kappa_i, \kappa_o$ ) and the ring-to-ring coupling coefficient  $\kappa_{N,2N}$ . The network is then reduced by one stage by computing  $S_{11}^{(N-1)}$  and  $S_{21}^{(N-1)}$ , and the process is repeated until the first stage,  $k = 1$ , is reached. The coupling coefficients of this stage can be obtained directly from the transfer functions of a pair of coupled microrings:  $\tau_1 = r_0^{(1)}$ ,  $\tau_2 = r_2^{(1)}$  and  $\kappa_3 = p_1^{(1)} / \kappa_1 \kappa_2$ .

### 4.2.3 A design example

As an illustrative example, we consider the design of an optical interleaver using a  $2 \times N$  coupled microring structure. Optical interleavers are a special class of optical devices that can be used to combine or separate the interleaved dense wavelength-division multiplexed signals on the even or odd channels. The device in this example is specified to have a 3dB bandwidth equal to half the free spectral range of the microrings, where  $\text{FSR} = 200\text{GHz}$ . The in-band ripples and stop-band rejection are specified to be better than 0.05dB and 30dB, respectively. Note that the device is very broadband as its 3dB bandwidth is half the FSR, so the microrings are expected to be very strongly coupled to each other. For this reason, the structure cannot be designed using the energy coupling formalism but requires a synthesis method based on the field coupling formalism in the  $z$ -domain.

$z^{-k}$	$P(z^{-1})$	$R(z^{-1})$	$Q(z^{-1})$
$k = 6$	0	0.110545	0.011908
5	0.145945	-0.380969	-0.078046
4	0.333375	0.723671	0.278279
3	0.454924	-0.888338	-0.439130
2	0.333375	0.723671	1.076002
1	0.145945	-0.380969	-0.435345
0	0	0.110545	1

Table 4.1. Coefficients of the transfer polynomials of the target filter response [46]

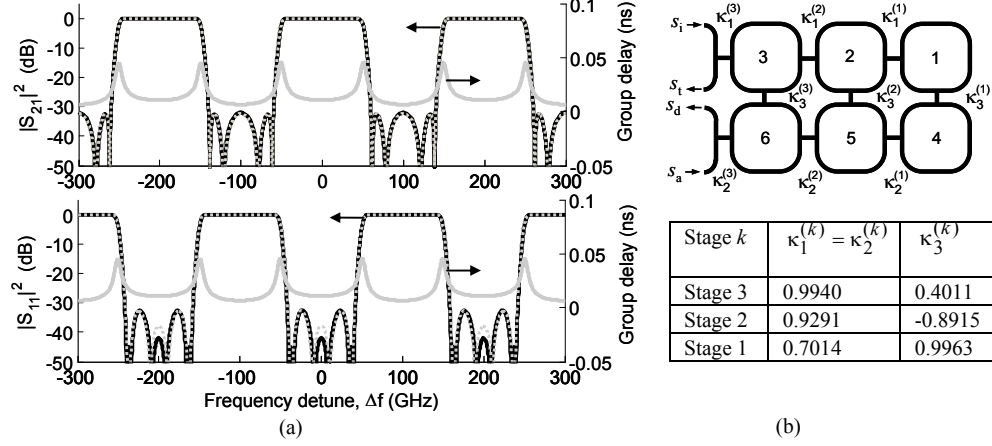


Figure 4.4. (a) Target (grey dotted lines) and synthesized (black solid lines) filter responses at the drop port ( $|S_{21}|^2$ ) and through port ( $|S_{11}|^2$ ). Grey solid lines show the group delay responses. (b) Schematic and coupling parameters of the synthesized CMR network. [46]

Using an appropriate filter approximation method (e.g., [44]), the transfer functions of a sixth-order filter satisfying the above specifications are obtained as given by the polynomials in Table 4.1. The target magnitude responses of  $S_{21}$  and  $S_{11}$  of the device are shown by the grey dotted lines in Figure 4.4(a).

The interleaver can be realized by a 2x3 CMR network, as shown in Figure 4.4(b). The coupling coefficients for each stage were computed using equations (4.42) and (4.44), and shown in the table in Figure 4.4(b). Since the device is very broadband, several coupling junctions have very large coupling values close to 1. To realize such strong couplings, the microrings should be designed to have long straight waveguide sections for coupling, as shown in Figure 4.4(b).

In Figure 4.4(a) we plotted the spectral responses of the synthesized CMR network (black solid lines), which are in good agreement with the target filter responses. Due to the very sharp roll-off of the filter, the transition band from the -0.5dB to -30dB attenuation point is only 12GHz, and the 0.5dB bandwidth extends as large as 96GHz, or 48% of the FSR. We also plotted the group delay response at each port in Figure 4.4(a) (grey solid lines), which shows that each channel has a relatively flat and small group delay of about 10ps at the center frequency. This example highlights a novel application of  $2 \times N$  CMR networks for realizing very compact interleavers.

### 4.3 Summary

In this chapter, we have presented two methods to synthesize a prescribed optical filter transfer function using two dimensional coupled microring resonator networks based on the field coupling formalism. The first method generates the field coupling matrix for the structure by solving the inverse of the analysis problem presented in Chapter 3. The method can be applied to general 2D coupling topologies; however, an approximation involving neglecting the indirect coupling matrix is required in order to construct the coupling topology from the field coupling matrix. The second method solves for the coupling coefficients exactly using the network order reduction technique and is applicable to  $2 \times N$  microring networks. Examples of advanced CMR optical filters were provided to illustrate the application of both methods in realizing prescribed optical transfer functions.

# Chapter 5

## Conclusions

In this thesis, we have presented a comprehensive analytic theory for the analysis and synthesis for two dimensional coupled microring resonator (2D CMR) networks based on the field coupling formalism. The techniques developed can be applied to strongly coupled CMRs for a wide range of applications in integrated optical filter analysis and design applications. A simple characteristic equation describing CMRs with general topologies allows closed form analytic expressions for the transmission characteristics to be derived. The theory developed characterizes the CMR structure through a field coupling matrix, which can be further decomposed into the direct and indirect coupling terms. It was found that the existing energy coupling formalism essentially makes the approximation that the indirect coupling term is negligible; such an approximation however is no longer valid under strong couplings between microrings and can have prominent effects on the device spectral characteristics. The field coupling formalism has the advantage over the existing energy coupling formalism in that it is no longer restricted to weakly-coupled microring networks, and is therefore suitable for analysis of broadband devices whose bandwidth becomes significant compared to its free spectral range.

Two methods for 2D CMR filter synthesis were also developed based on the field coupling formalism. One synthesis method is based on the inverse of the analysis problem and has the advantage of maintaining generality of the coupling topologies, but still requires some approximations in the determination of the coupling coefficients. The other method is based on the network order reduction approach and synthesizes the CMR network directly stage by stage, but it is limited to the  $2 \times N$  coupling topology.

## **5.1 Major contributions**

Major achievements of the work could be summarized as the following:

- Formulated a general theoretical framework for the analysis of general 2D CMR structures based on the field coupling formalism;
- Investigated novel effects in strongly coupled CMR structures such as the effects of indirect couplings;
- Developed two CMR filter synthesis techniques based on the field coupling formalism;
- Demonstrated advanced applications of strongly coupled microring resonator networks in realizing broadband integrated optical filters.

## **5.2 Recommendations for future works**

While the presented work provides a comprehensive theoretical framework for the coupled microring resonators, there are still rooms for improvements and

further investigations in the following areas:

- Search for a novel solution to remove the final approximation in the general synthesis approach;
- Validate the analytical spectral responses obtained with the field coupling formalism by comparing them to rigorous full-wave simulations of 2D CMR networks;
- Explore feasibility of experimentally realizing 2D CMR filter designs;
- Extend the field coupling theory developed to non-linear 2D CMR networks.

# Bibliography

---

- [1] B. E. Little, S. T. Chu, P. P. Absil, J. V. Hryniewicz, F. G. Johnson, F. Seiferth, D. Gill, V. Van, O. King and M. Trakalo, "Very high-order microring resonator filters for WDM applications", *IEEE Photon. Technol. Lett.*, vol. 16, pp. 2263-2265, 2004.
- [2] A. Melloni, F. Morichetti and M. Martinelli, "Linear and nonlinear pulse propagation in coupled resonator slow-wave optical structures", *Opt. Quantum. Electron.*, vol. 35, pp. 365-379, 2003.
- [3] F. Xia, L. Sekaric and Y. Vlasov, "Ultracompact optical buffers on a silicon chip", *Nat. Photon.*, vol. 1, pp. 65-71, 2007.
- [4] D. D. Smith, H. Chang, K. A. Fuller, A. T. Rosenberger and R. W. Boyd, "Coupled-resonator-induced transparency", *Phys. Rev. A*, vol. 69, 063804, 2004.
- [5] V. Van, "Synthesis of elliptic optical filters using mutually coupled microring resonators", *J. Lightw. Technol.*, vol. 25, pp. 584-590, 2007
- [6] V. Van, "Advanced coupled-micro-resonator architectures for dispersion and spectral engineering applications", *Proc. SPIE*, 721906, 2009.
- [7] K. Jinguji, "Synthesis of coherent two-port optical delay-line circuit with ring waveguides," *J. Lightwave Technol.*, vol. 14, pp. 1882-1898, 1996.

- [8] C.K. Madsen, "Efficient architectures for exactly realizing optical filters with optimum bandpass design," *IEEE Photon. Technol. Lett.*, vol. 10, pp. 1136-1138, 1998.
- [9] R. Orta, P. Savi, R. Tascone and D. Trincherro, "Synthesis of multiple-ring-resonator filters for optical systems", *IEEE Photon. Technol. Lett.*, vol. 7, no. 12, pp. 1447-1449, 1995.
- [10] B.E. Little, S.T. Chu, H.A. Haus, J. Foresi, and J-P. Laine, "Microring resonator channel dropping filters," *J. Lightwave Technol.*, Vol. 15, No. 6, pp. 998-1005, 1997.
- [11] B.E. Little, S.T. Chu, J.V. Hryniewicz and P.P. Absil, "Filter synthesis for periodically coupled microring resonators," *Opt. Lett.*, vol. 25, pp. 344-346, 2000
- [12] R. Grover, V. Van, T.A. Ibrahim, P.P. Absil, L.C. Calhoun, F.G. Johnson, J.V. Hryniewicz and P-T. Ho, "Parallel-cascaded semiconductor microring resonators for high-order and wide-FSR filters," *J. Lightwave Technol.*, vol. 20, pp. 900 - 905, 2002.
- [13] Y. M. Landobasa, S. Darmawan and M.-K. Chin, "Matrix analysis of 2-D microresonator lattice optical filters," *IEEE J. Quantum. Electron.*, vol. 41, no. 11, pp. 1410-1418, 2005.
- [14] V. Van, "Dual-Mode Microring Reflection Filters," *J. Lightwave Technol.* Vol. 25, No. 10, pp. 3142-3150, 2007.
- [15] V. Van, "Canonic Design of Parallel Cascades of Symmetric Two-Port Microring networks," *J. Lightwave Technol.* Vol. 27, No. 21, pp. 4870-4877, 2009.

- [16] J. K. S. Poon, J. Scheuer, S. Mookherjea, G. T. Paloczi, Y. Huang and A. Yariv, "Matrix analysis of microring coupled-resonator optical waveguides," *Opt. Express*, vol. 12, pp. 90-103, 2004.
- [17] H. L. Liew and V. Van, "Exact realization of optical transfer functions with symmetric transmission zeros using the double-microring ladder architecture", *J. Lightw. Technol.*, vol. 26, pp. 2323-2331, 2008.
- [18] I. Chremmos and N. Uzunoglu, "Modes of the infinite square lattice of coupled microring resonators", *J. Opt. Soc. Am. A*, vol. 25, no. 12, pp. 3043-3050, 2008.
- [19] M. Gad, D. Yevick and P. Jessop, "Compound ring resonator circuit for integrated optics applications", *J. Opt. Soc. Am. A*, vol. 26, no. 9, pp. 2023-2032, 2009.
- [20] J. K. S. Poon, J. Scheuer, Y. Xu and A. Yariv, "Designing coupled-resonator optical waveguide delay lines", *J. Opt. Soc. Am. B*, vol. 21, no. 9, pp. 1665-1673, 2004.
- [21] W. Chen, Z. Wang, W. Chen and Y.-J. Chen, "General ring-resonator analysis and characterization by characteristic matrix", *J. Lightw. Technol.*, vol. 23, no. 2, pp. 915-922, 2005.
- [22] D. Marcuse, "Theory of Dielectric Optical Waveguides," 2nd ed. Academic, New York, 1991.
- [23] W-P. Huang, "Coupled-mode theory for optical waveguides: an overview" *JOSA A*, Vol. 11, Issue 3, pp. 963-983, 1994.
- [24] V. Van, M. A. Prabhu, "Multiple coupled microresonator devices for advanced spectral shaping applications," *Proc. SPIE Vol. 6872, 68720S* (2008)

- [25] A.E. Williams, W.G. Bush, R.R. Bonetti, "Predistortion techniques for multicoupled resonator filters," *IEEE Trans. Microwave Theory Tech.*, Vol. 33, Issue 5, pp. 402-407, 1985
- [26] M. Gad, D. Yevick, and P. Jessop, "A comparison of modeling methods for ring resonator circuits," *J. Opt. Soc. Am. A*, vol. 27, no. 4, pp. 703-708, 2010.
- [27] R. Orta, P. Savi, R. Tascone and D. Trincherro, "Synthesis of multiple-ring-resonator filters for optical systems", *IEEE Photon. Technol. Lett.*, vol. 7, no. 12, pp. 1447-1449, 1995.
- [28] J. K. S. Poon, J. Scheuer, S. Mookherjea, G. T. Paloczi, Y. Huang and A. Yariv, "Matrix analysis of microring coupled-resonator optical waveguides", *Opt. Express*, vol. 12, pp. 90-103, 2004.
- [29] Y. M. Landobasa, S. Darmawan and M.-K. Chin, "Matrix analysis of 2-D microresonator lattice optical filters", *IEEE J. Quantum. Electron.*, vol. 41, no. 11, pp. 1410-1418, 2005.
- [30] A. Tsay and V. Van, "Strongly coupled microring resonators and the effect of non-adjacent resonator coupling," presented in *IEEE Photon. Soc. Annual Meeting 2010*, Denver, CO, USA, paper no. WI4
- [31] A. Tsay and V. Van, "Analytic Theory of Strongly-Coupled Microring Resonators," *IEEE J. Quantum Electron.*, vol. 47, no. 7, pp. 997-1005, 2011
- [32] M. Marcus and H. Minc, "A Survey of Matrix Theory and Matrix Inequalities", Boston: Allyn and Bacon Inc., 1964.
- [33] M.A. Popovic, C. Manolatu and M.R. Watts, "Coupling-induced resonance frequency shifts in coupled dielectric multi-cavity filters," *Optics Express*, vol. 14, no. 3, pp. 1208-1222, 2006

- [34] S. V. Boriskina, "Photonic molecules and spectral engineering," *Photonic Microresonator Research and Applications* (Eds. I. Chremmos, O. Schwelb, N. Uzunoglu). New York: Springer, 2010.
- [35] Y. Hara, T. Mukaiyama, K. Takeda and M. Kuwata-Gonokami, "Photonic molecule lasing", *Opt. Lett.*, vol. 28, no. 24, pp. 2437-2439, 2003.
- [36] M. J. Hartmann, F. G. S. L. Brandao, "Strongly interacting polaritons in coupled arrays of cavities", *Nat. Phys.*, vol. 2, pp. 849 – 855, 2006.
- [37] H. Lin, J.-H. Chen, S.-S. Chao, M.-C. Lo, S.-D. Lin and W.-H. Chang, "Strong coupling of different cavity modes in photonic molecules formed by two adjacent microdisk cavities", *Opt. Express*, vol. 18, no. 23, pp. 23948-23956, 2010.
- [38] F. Casas and A. Murua, "An efficient algorithm for computing the Baker-Campbell-Hausdorff series and some of its applications", *J. Math. Phys.*, vol. 50, 033513, 2009.
- [39] A. Tsay and V. Van, "Analytical Method for Designing Strongly Coupled Microring Resonator Networks," presented at Integrated Photonics Research, Silicon and Nano Photonics (IPR) Topical Meeting, Toronto, ON, Canada, Jun 12-16, 2011. Paper IWD3.
- [40] C.J. Kaalund and G-D. Peng, "Pole-Zero Diagram Approach to the Design of Ring Resonator-Based Filters for Photonic Applications," *J. Lightw. Technol.*, Vol. 22, No. 6, pp. 1548-1559, 2004
- [41] M.A. Swillam, O.S. Ahmed, M.H. Bakr, and X. Li, "Filter Design Using Multiple Coupled Microcavities," *IEEE Photon. Tech. Lett.*, VOL. 23, NO. 16, pp. 1060-1162, 2011
- [42] V. Belevitch, "Classical Network Theory," San Francisco, CA, 1968

- [43] V. Van, "Advanced microring photonic filter design," Photonic Microresonator Research and Applications, Springer Series in Optical Sciences, vol. 156, pp. 115-138, 2010
- [44] H.G. Martinez and T.W. Parks, "Design of recursive digital filters with optimum magnitude and attenuation poles on the unit circle," IEEE Trans. Acoustics, Speech Signal Proc., vol. ASSP-26, no. 2, pp. 150-156, 1978
- [45] A.M. Prabhu, H.L. Liew and V. Van, "Generalized parallel-cascaded microring networks for spectral engineering applications," J. Opt. Soc. Am. B, vol. 25, no 9, pp. 1505-1514, 2008
- [46] A. Tsay and V. Van, "A Method for Exact Synthesis of  $2 \times N$  Coupled Microring Resonator Networks," to appear in IEEE Photon. Technol. Lett. , 2011.